

# Bayesian Semiparametric Longitudinal Drift-Diffusion Mixed Models for Tone Learning in Adults

Giorgio Paulon<sup>1</sup> (giorgio.paulon@utexas.edu)  
 Fernando Llanos<sup>2</sup> (f.llanos@pitt.edu)  
 Bharath Chandrasekaran<sup>2</sup> (b.chandra@pitt.edu)  
 Abhra Sarkar<sup>1</sup> (abhra.sarkar@utexas.edu)

<sup>1</sup>Department of Statistics and Data Sciences,  
 University of Texas at Austin,  
 2317 Speedway (D9800), Austin, TX 78712-1823, USA

<sup>2</sup>Department of Communication Sciences and Disorders,  
 University of Pittsburgh,  
 4028 Forbes Tower, Pittsburgh, PA 15260, USA

## Abstract

Understanding how the adult humans learn to to categorize novel auditory categories is an important problem in auditory behavioral neuroscience. Drift diffusion models are popular, neurobiologically relevant approaches to assess the mechanisms underlying speech learning. Motivated by these problems, we develop a novel inverse-Gaussian drift-diffusion mixed model for multi-alternative decision making processes in longitudinal settings. Our methodology builds on a novel Bayesian semiparametric framework for longitudinal data in the presence of a categorical covariate that allows automated assessment of the predictor's local time-varying influences. We design a Markov chain Monte Carlo algorithm for posterior computation. We evaluate the method's empirical performances through synthetic experiments. Applied to a speech category learning data set, the method provides novel insights into the underlying mechanisms.

**Key Words:** Auditory neuroscience, B-splines, Drift-diffusion models, (Factorial) hidden Markov models, Functional models, Inverse-Gaussian distributions, Local clustering, Longitudinal mixed models, Perceptual decision making, Speech perception neuroscience, Speech learning in adults, Wiener processes

**Short/Running Title:** Longitudinal Drift-Diffusion Mixed Models

**Corresponding Author:** Abhra Sarkar (abhra.sarkar@utexas.edu)

# 1 Introduction

Understanding the cognitive and biological mechanisms underlying our ability to learn new speech categories constitute important questions in auditory neuroscience. The inherent dynamic complexities are not well understood yet, and they are being studied through extensive ongoing research.

The research reported here is motivated particularly by experiments on the acquisition of Mandarin tones by native speakers of English. Native speech categories are acquired during the first year of life, within a so-called phonetic sensitivity period. There is a neural commitment to native-language speech sounds, and that this commitment may preclude the learning of novel speech categories in adulthood (Johnson and Newport, 1989; Iverson *et al.*, 2003). In Mandarin, there are four tone categories that systematically change word meaning. These tones are, however, linguistically irrelevant in English. English native speakers thus struggle to generalize their differences (Wang *et al.*, 1999; Chandrasekaran *et al.*, 2010; Maddox and Chandrasekaran, 2014). In laboratory settings, combining exposure to perceptually variable tones with trial-by-trial corrective feedback can improve tone categorization skills within a few hundred trials. Reaching a native like proficiency, however, may take several sessions of training (Xie *et al.*, 2017; Reetzke *et al.*, 2018). The perceptual and sensory representation of Mandarin tones gets fundamentally refined over the course of this learning period (Feng *et al.*, 2018). Understanding this longitudinal evolution is critical to assess the cognitive dynamics of speech category learning. The statistical challenge is to make this assessment from behavioral data on tone categorization responses and response times.

To this end, we can identify the Mandarin tone categorization problem with the broader class of problems of multi-category decision making under perceptual stimuli (Smith and Ratcliff, 2004; Heekeren *et al.*, 2004; Gold and Shadlen, 2007; Schall, 2001; Purcell, 2013; Glimcher and Fehr, 2013). In such contexts, drift-diffusion processes are popular models for behavioral accuracies and response times as they mimic the accumulation of evidence in favor of different decision alternatives in the human brain (Ratcliff, 1978; Ratcliff *et al.*, 2016). The existing literature on drift-diffusion models is substantive but also heavily focused on the two category case with a single latent diffusion process with two boundaries, one for each of the two decision alternatives (Smith and Vickers, 1988; Ratcliff and Rouder, 1998; Ratcliff and McKoon, 2008). The joint likelihood of the accuracies and response times under such models is mathematically complex and computationally expensive (Navarro and Fuss, 2009; Tuerlinckx, 2004; Tuerlinckx *et al.*, 2001). Inference in such models is thus often based on approximations of the likelihood (Vandekerckhove and Tuerlinckx, 2007), or on the conditional likelihood of the response times, conditioned on the decisions (Vandekerckhove *et al.*, 2008). Multi-category drift-diffusion models with separate latent processes, one for each decision category and simultaneously at play, have been

developed to address some of the limitations (Usher and McClelland, 2001; Brown and Heathcote, 2008; Leite and Ratcliff, 2010; Dufau *et al.*, 2012), but the literature remains sparse with methods available only for simple static design settings.

Learning to distinguish Mandarin tones and more generally to make categorization decisions are, however, dynamic processes, driven by continuous and nuanced perceptual adjustments in our brain and behavior over time. Existing models are thus severely limited in their ability to capture the true inherent complexities, including assessing the biologically relevant changes that take place over the learning period. Principled statistical approaches to dynamic drift-diffusion mixed effects models, that appropriately accommodate fixed effects of experimental factors as well as random effects due to subjects, are therefore highly needed but present daunting methodological and computational challenges. In this article, we address these challenges by developing a biologically interpretable flexible Bayesian semiparametric drift-diffusion mixed model for studying multi-alternative perceptual decision making processes in longitudinal settings.

Our methodology builds on a novel statistical framework for longitudinal mixed models in the presence of categorical covariates. Such settings may be viewed as longitudinal adaptations of static ANOVA designs and are frequently encountered in modern research in diverse scientific fields. In our motivating auditory neuroscience example, for instance, the different input tones and the associated response categories constitute the levels of a categorical predictor.

The construction of our longitudinal mixed model framework proceeds by characterizing the longitudinal evolution of both the predictor dependent fixed effects and the subject specific random effects as flexible smooth functions of time (Ramsay and Silverman, 2007; Morris, 2015; Wang *et al.*, 2016) modeled by mixtures of locally supported spline bases (de Boor, 1978; Eilers and Marx, 1996). The fixed effects model spline coefficients vary with the associated predictor levels. Dependence across adjacent temporal locations is further induced via hidden Markov models (HMMs) (McDonald and Zucchini, 1997; Rabiner, 1989; Frühwirth-Schnatter, 2006; Cappé *et al.*, 2005) for the latent cluster indicator variables and novel Markovian priors on the core spline coefficients. The HMMs, adapted in such novel ways, induce a local clustering mechanism for the predictor categories, enabling the assessment of their varying temporal influences while also reducing model dimensionality.

We adapt our proposed framework to develop a longitudinal multi-category inverse-Gaussian drift-diffusion mixed model that allows the model parameters to evolve flexibly over time as the participants get more experience and training in their decision tasks. To our knowledge, the inverse-Gaussian drift-diffusion model is itself novel to the literature. Importantly, as a direct consequence of the local cluster inducing mechanism built into the longitudinal framework, the perceptual stimuli are allowed to affect the underlying diffusion processes differently at different longitu-

dinal stages of the experiment. This allows us to assess scientifically relevant local differences in the underlying mechanisms in different learning phases.

The literature on longitudinal data analysis models is enormous. See, for example, books by Diggle *et al.* (2002); Singer *et al.* (2003); Fitzmaurice *et al.* (2008) and the references therein. Bayesian methods for longitudinal data have also been extensively developed (Daniels and Pourahmadi, 2002; Chib and Hamilton, 2002; Li *et al.*, 2010; Müller *et al.*, 2013; Quintana *et al.*, 2016, etc.). The problem of modeling temporally varying predictor influences has, however, not garnered much attention. We can only mention Petrone *et al.* (2009); Nguyen and Gelfand (2011, 2014), all of which were designed primarily for normally distributed functional data with continuous covariates. It is not clear how these approaches can be adapted to our problem.

The novel longitudinal mixed model framework proposed here is highly generic and broadly adaptable and may thus be of independent interest to the statistics community. Its workings are perhaps better understood when introduced separately from drift-diffusion models, which bring in many additional layers of complexities and challenges, as we do here. To keep the focus of this article on drift-diffusion mixed models and perceptual decision making, a more rigorous study of the proposed generic mixed model framework in simpler likelihood settings is being pursued separately elsewhere (Paulon and Sarkar, 2020).

Overall, our proposed longitudinal multi-category inverse-Gaussian drift-diffusion mixed model takes the existing state-of-the-art many significant steps forward, including (a) introducing a novel biologically interpretable class of inverse-Gaussian drift-diffusion models for decision making, (b) accommodating fixed effects of perceptual stimuli and random effects due to subject specific heterogeneity in such models in a statistically principled manner, (c) adapting these models to longitudinal study designs, enabling the study of the temporal evolution of underlying process parameters as the subjects get trained and experienced in their assigned decision tasks, (d) allowing the process parameters to be locally clustered, enabling automated assessment of the local similarities and differences of the decision making mechanisms in various learning stages. The methods proposed here thereby allow scientists to study perceptual decision making processes at levels much finer than previously conceivable.

The rest of this article is organized as follows. Section 2 provides additional background on tone learning and drift-diffusion models. Section 3 develops the generic mixed model longitudinal framework. Section 4 then builds on this and develops the longitudinal drift-diffusion mixed model. Section 5 outlines computational challenges and solution strategies. Section 6 presents the results of the proposed method applied to tone learning data. Section 7 presents the results of simulation experiments. Section 8 contains concluding remarks. Substantive additional details, including Markov chain Monte Carlo (MCMC) based posterior inference algorithms, are deferred to the supplementary materials.

## 2 Behavioral Data and Background

The behavioral data set that motivated our research comes from an intensive multi-day longitudinal speech category training study reported previously in Reetzke *et al.* (2018). In this study,  $n = 20$  native English-speaking adults were trained to categorize Mandarin Chinese syllables into lexical tone categories as a function of their pitch contour. Mandarin Chinese has four syllabic pitch contours or tones that are used to convey different lexical meanings. For example, in Mandarin Chinese, the syllable ‘ma’ can be interpreted as ‘mother’, ‘hemp’, ‘horse’, or ‘scold’ depending on whether is pronounced with a high-level (T1), low-rising (T2), low-dipping (T3), or high-falling (T4) tone, respectively. The stimuli consisted of these tones pronounced by four native Mandarin speakers. The trials were administered in homogeneous blocks. Each block comprised 40 categorization trials for 40 different speech exemplars, corresponding to different combinations of speakers, syllables, and input tones. Participants were trained across several days, with five blocks on each day. On each categorization trial, participants indicated the tone category they heard via button press on a computer keyboard. Following the button press, they were given corrective feedback (‘Correct’ / ‘Incorrect’) on a computer screen. Individual categorization performance was monitored across training sessions until each participant achieved and maintained accuracy levels comparable to that of native speakers of Mandarin.

The data consist of proportions of times the different tones were identified and associated response times for different input tones for the 20 participants. We focus here on the first two days of training (10 blocks in total) as they exhibited the steepest improvement in learning as well as striking individual differences relative to any other collection of blocks (Figure 1). In that sense, they provide an optimal longitudinal frame to assess the effects of learning on decision making variables.

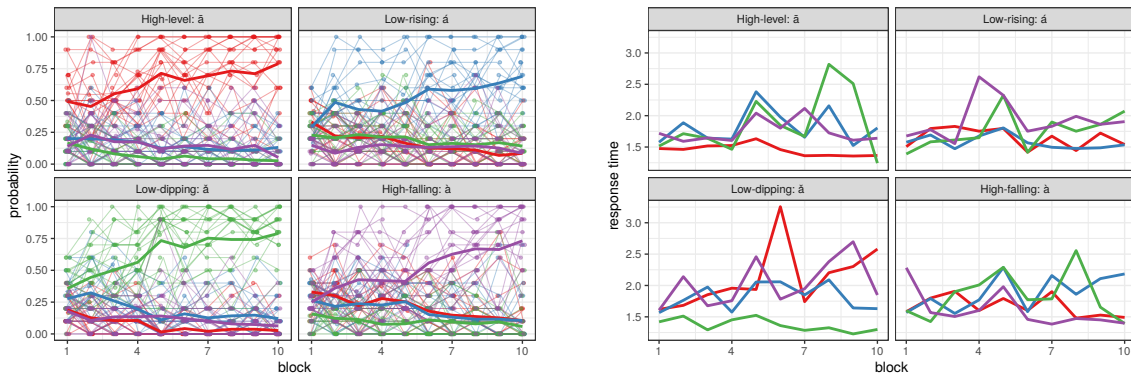


Figure 1: Left panel: proportions of times an input tone was classified into different tone categories by different subjects. The thick line represents the average performance across subjects for clarity. Right panel: associated response times averaged across subjects for clarity. In both panels, high-flat tone responses are shown in red; low-rising in blue; low-dipping in green; and high-falling in purple.

The tone identification problem can be viewed from a broader perspective of multi-category decision making tasks under perceptual stimuli, and hence can be studied using computational models developed for such tasks. We present here a brief non-technical overview of how these models relate to the underlying neurobiology. Mathematical details and developments are deferred to Section 4. A more detailed review of the neural mechanisms specific to speech learning processes can be found in Section S.1 of the supplementary materials.

In a typical multi-category decision task, the brain accumulates sensory evidence in support of each choice. This accumulation process is reflected in increasing firing rate at local neural populations associated with different decisions. The decision is taken when neural activity at one of these populations reaches a particular threshold level. Here, the decision that is taken is predictable from the decision threshold that is crossed first (Gold and Shadlen, 2007; Brody and Hanks, 2016).

Changes in evidence accumulation rates and decision thresholds can be induced by task difficulty or cognitive impairment affecting neural activity in the brain (Cavanagh *et al.*, 2011; Ding and Gold, 2013). Decision-making is also regulated by demands on both speed and accuracy as a function of the task (Bogacz *et al.*, 2010; Milosavljevic *et al.*, 2010). Separate models for accuracies (Paulon *et al.*, 2019) and response times (Craigmile *et al.*, 2010) cannot provide a meaningful interpretation of this speed-accuracy trade-off.

An excellent basis for jointly modeling accuracies and response times is obtained by imitating the underlying neural evidence accumulation mechanisms via latent drift-diffusion processes racing toward their respective boundaries, the process reaching its boundary first producing the final observed decision and the time taken to reach this boundary giving the associated response time (Figure 2) (Usher and McClelland, 2001). The drift and the boundary parameters jointly explain the dynamics of choice, including the speed-accuracy trade-off. Decision thresholds remaining fixed, higher drift rates for the correct perceptual stimuli lead to faster and more accurate responses. For fixed drift rates, on the other hand, lower decision thresholds decrease response times at the expense of accuracy.

In our motivating tone learning experiment, we are interested in understanding the longitudinal evolution of the underlying drift-diffusion processes as the participants gain more training and experience in identifying the tones over time. Importantly, we are not only interested in assessing the global influences of the input perceptual stimuli but also if they might be affecting the underlying processes differently at different longitudinal stages of the experiment. The novel locally varying longitudinal functional mixed model framework developed in Section 3 provides a crucial building block toward that goal.

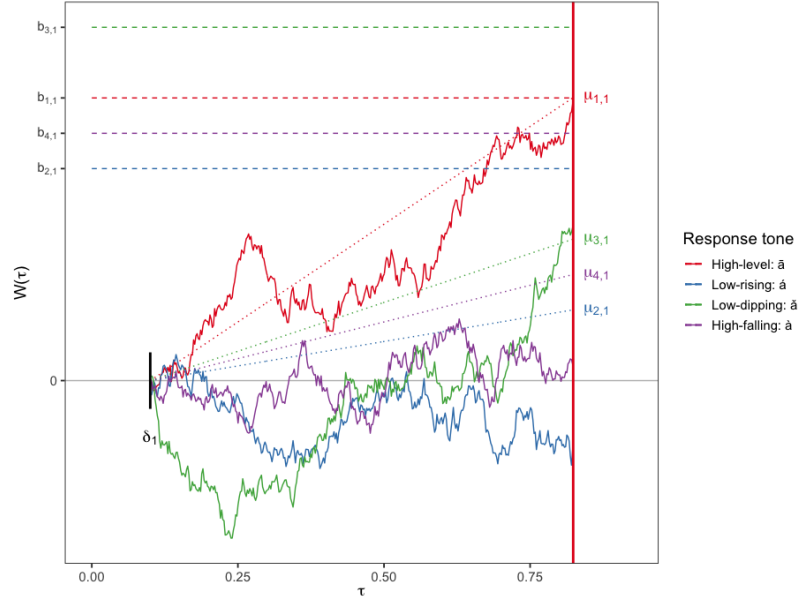


Figure 2: Drift-diffusion model for perceptual decision making. After an initial  $\delta_s$  amount of time required to encode an input signal  $s$ , the evidence in favor of a response category  $d$  accumulates according to a Wiener diffusion process with drift  $\mu_{d,s}$ . The decision  $d$  is eventually taken if the underlying process is the first to reach its decision boundary  $b_{d,s}$ . Here we illustrate a tone learning trial with input tone T1 that was eventually correctly identified. Section 2 provides additional neurobiological background. Section 4 provides additional mathematical details.

### 3 Longitudinal Functional Mixed Models

In this section, we develop a novel statistical framework for mixed effects  $\theta_x^{(i)}(t)$  generated under the influence of a categorical predictor  $x \in \mathcal{X} = \{1, \dots, c_x\}$  longitudinally over time  $t$ . To be more precise, responses  $y_{i,\ell,t_i}$ , available for  $i \in \{1, \dots, n\}$  individuals and  $\ell \in \{1, \dots, m_{i,t_i}\}$  trials at  $t_i \in \{t_{i,1}, \dots, t_{i,T}\}$  time points, are generated under the influence of the predictor  $x_{i,\ell,t_i}$  as

$$\begin{aligned} \{y_{i,\ell,t} \mid x_{i,\ell,t} = x, \theta_x^{(i)}(t), \theta_\epsilon\} &\sim f_y\{y_{i,\ell,t} \mid \theta_x^{(i)}(t), \theta_\epsilon\}, \\ \theta_x^{(i)}(t) &= f_x(t) + u_i(t), \quad u_i(t) \sim f_u\{u_i(t) \mid \theta_u\}, \end{aligned} \tag{1}$$

where  $f_y$  is the likelihood function with mixed effects parameters  $\theta_x^{(i)}(t)$  and separate additional parameters  $\theta_\epsilon$ ,  $f_x(t)$  denotes time-varying fixed effects due to  $x$ ,  $u_i(t)$  are time-varying random effects due to the  $i^{th}$  subject, and  $f_u$  is the random effects distribution with parameters  $\theta_u$ . When multiple categorical predictors  $x_j \in \mathcal{X}_j = \{1, \dots, c_j\}$ ,  $j = 1, \dots, p$  are available, the proposed approach extends conceptually

straightforwardly by defining  $x = (x_1, \dots, x_p)^T$  with  $\mathcal{X} = \mathcal{X}_1 \times \dots \times \mathcal{X}_p$ .

Importantly, we are not only interested in assessing the overall global influence of  $x$  on  $f_x(t)$  also how its levels influence  $f_x(t)$  locally at various temporal stages of the longitudinal study. The problem is of direct relevance to our motivating auditory neuroscience tone categorization experiments, where we are interested in understanding the local similarities and dissimilarities between the decision making neural mechanisms under different perceptual stimuli as the participants gain more training and experience longitudinally over time. Additionally, we are not just interested in estimating population level effects but also how the mechanisms vary across the participants.

For ease of exposition, we assume henceforth that the data points are all measured at a common set of equidistant time points, denoted simply as  $\{1, \dots, T\}$ . Also, an equal number  $L$  of trials is conducted per individual at each time point, that is,  $\ell \in \{1, \dots, L\}$ . This is certainly the case for our motivating tone categorization application. The methodology we develop here extends conceptually straightforwardly to scenarios with unequal numbers of trials and/or unequally spaced time points. To simplify notation, with some abuse, generic data recording time stamps as well as other generic time points in our domain of interest will both be denoted by  $t$ . Likewise, the covariate and its levels will both be denoted by  $x$  and so forth.

### 3.1 Locally Varying Fixed Effects

We propose a novel approach to modeling the latent functions  $f_x(t)$  using basis decomposition methods that allow them to smoothly vary with time  $t$  while also locally depend on the predictor levels  $x$ . Specifically, we let

$$f_x(t) = \sum_{k=1}^K \beta_{k,x} b_k(t), \quad (2)$$

where  $\mathbf{b}(t) = \{b_1(t), \dots, b_K(t)\}^T$  are a set of known locally supported basis functions and  $\boldsymbol{\beta}_x = \{\beta_{1,x}, \dots, \beta_{K,x}\}$  are unknown coefficients to be estimated from the data. In this article, we use B-spline bases which are nonnegative, continuous and have the desirable local support properties (Figure 3). Mixtures of B-splines are highly flexible (de Boor, 1978). Allowing the  $\beta_{k,x}$ 's to flexibly vary with  $x$ , the model can also accommodate widely different behavior for different predictor levels.

It is difficult to assess the influences of the predictor using such unstructured models. A potentially efficient solution that reduces dimensions while also facilitating the assessment of the importance of the predictor is to cluster the parameters by allowing them to have common shared values across different predictor levels. If, for example,  $\boldsymbol{\beta}_{x_1} = \boldsymbol{\beta}_{x_2}$  for two levels  $x_1$  and  $x_2$  of  $x$ , then not only have we reduced the number of parameters to be modeled and hence improved the efficiency in estimating



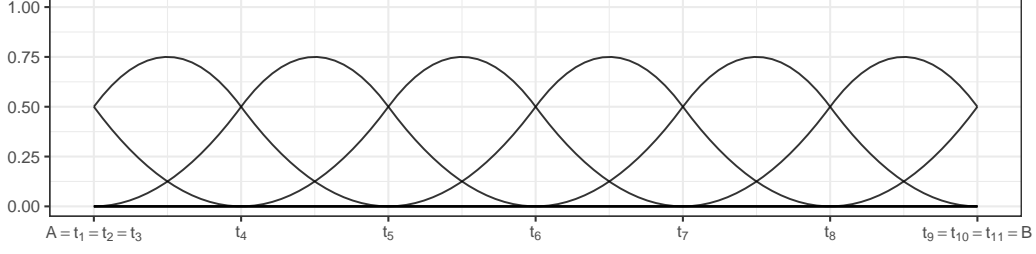


Figure 3: Plot of 9 quadratic B-splines on an interval  $[A, B]$  defined by 11 equidistant knot points that divide  $[A, B]$  into  $K = 6$  equal subintervals.

these parameters but have also established that the two levels  $x_1$  and  $x_2$  of  $x$  have no differential effect on the data generating mechanism.

For many practical applications, however, such global clustering of all elements of  $\beta_x$  together will be restrictive. It is also difficult to assess local influences of the predictor using such strategy. More realistically, the elements of  $\beta_x$  should be allowed to cluster locally. With  $\mathcal{K} = \{1, \dots, K\}$ ,  $\beta_{k,x}$  may, for example, vary with  $x$  at locations  $k \in \mathcal{K}_v \subset \mathcal{K}$  but may be shared across several combinations of  $x$  at the remaining locations  $k \in \mathcal{K}_c = \mathcal{K} - \mathcal{K}_v$ . To induce such local clustering, we introduce latent variables  $z_k^{(x)} \in \mathcal{X} = \{1, \dots, c_x\}$  and let

$$\{f_x(t) \mid z_k^{(x)} = z_k\} = \sum_{k=1}^K \beta_{k,z_k}^* b_k(t), \quad (3)$$

or equivalently,  $(\beta_{k,x} \mid z_k^{(x)} = z_k) = \beta_{k,z_k}^*$ .

The set of B-spline coefficients to be estimated at the  $k^{th}$  location now comprises the  $\beta_{k,z_k}^*$ 's that are indexed with  $z_k^{(x)} = z_k$  at that location  $k$ . More precisely, letting

$$\mathcal{Z}_k = \{z_k : z_k^{(x)} = z_k \text{ for some } x \in \mathcal{X}\} \quad \text{and} \quad \mathcal{B}_k^* = \{\beta_{k,z_k}^* : z_k \in \mathcal{Z}_k\},$$

the set of B-spline coefficients to be estimated at location  $k$  is  $\mathcal{B}_k^*$ . Clearly,  $|\mathcal{B}_k^*| = |\mathcal{Z}_k|$ . When the  $z_k^{(x)}$ 's are assigned probability models supported on  $\mathcal{X}$ , the number of distinct values taken on by the  $z_k^{(x)}$ 's, namely  $|\mathcal{Z}_k| = \ell_k$  say, may be less than  $|\mathcal{X}| = c_x$ . The effective size of the coefficient space  $\mathcal{B}_k^*$  at location  $k$  is thus  $|\mathcal{B}_k^*| = |\mathcal{Z}_k| = \ell_k \leq c_x = |\mathcal{X}|$ . Significant reduction in dimension is thus achieved when  $\sum_{k=1}^K \ell_k \ll K c_x$ .

When  $z_k^{(x_1)} = z_k^{(x_2)}$  for two different levels  $x_1$  and  $x_2$  of  $x$ , the spline coefficients at location  $k$  do not differ between  $x_1$  and  $x_2$ . There is thus no significant difference between how the two levels  $x_1$  and  $x_2$  influence the response  $y$  at location  $k$ . Importantly thus, the case  $|\mathcal{Z}_k| = 1$  characterizes the scenario when  $x$  has no influence on  $y$  at location  $k$ . On the other end, when  $|\mathcal{Z}_k| = c_x$ , the  $z_k^{(x)}$ 's take on different values for

different levels of  $x$ , implying that the spline coefficients are all different for different levels of  $x$  at location  $k$ . All levels of  $x$  now significantly differently influence the response generating mechanism at location  $k$ . In many practical applications,  $|\mathcal{Z}_k|$  will tend to be much smaller than  $c_x$  and the restriction  $z_k^{(x)} \in \mathcal{Z} = \{1, \dots, z_{\max}\} \subset \mathcal{X}$  with  $z_{\max} < c_x$  will suffice.

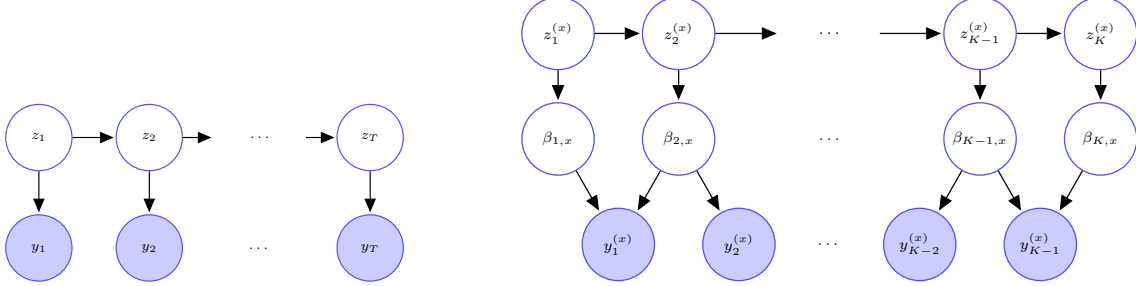


Figure 4: Left panel: Graph of a conventional HMM. Right panel: Graph of our proposed functional HMM model (3) with quadratic B-splines (Figure 3) with knots points at the data generating time stamps ( $T = K - 1$ ).

We now consider the problem of specifying probability models for the  $z_k^{(x)}$ 's and the  $\beta_{k,z_k}^*$ 's, accommodating temporal dependencies across  $k$ . We model the temporal evolution of the latent local cluster indicators  $z_k^{(x)}, k = 1, \dots, K$ , using hidden Markov models (HMM) as

$$(z_k^{(x)} \mid z_{k-1}^{(x)} = z_{k-1}) \sim \text{Mult}(\pi_{z_{k-1},1}^{(x)}, \dots, \pi_{z_{k-1},z_{\max}}^{(x)}).$$

When the  $z_k^{(x)}$ 's corresponding to two different categories of  $x$  are equal in a temporal region, the local support properties of B-splines then cause the underlying curves to be the same in that region. If, on the contrary, the  $z_k^{(x)}$ 's corresponding to two different values of  $x$  are different, the underlying curves there will also be different. We assign hierarchical Dirichlet priors on the transition probabilities

$$\boldsymbol{\pi}_z^{(x)} = (\pi_{z,1}^{(x)}, \dots, \pi_{z,z_{\max}}^{(x)})^T \sim \text{Dir}(\alpha_x/z_{\max}, \dots, \alpha_x/z_{\max}) \quad \text{with} \quad \alpha_x \sim \text{Ga}(a, b).$$

In what follows, we refer to this model as a functional HMM. In contrast to conventional HMMs, where the cluster specific atoms  $\beta_z$  are shared across locations  $k$ , in the proposed functional HMM, the atoms  $\beta_{k,z}$  are different at different locations  $k$ .

We next consider priors for the atoms  $\beta_{k,z_k}^*$ . Conditional on the  $z_k^{(x)}$ 's and the coefficients at the previous locations, for  $k = 2, \dots, K$ , we construct the priors se-

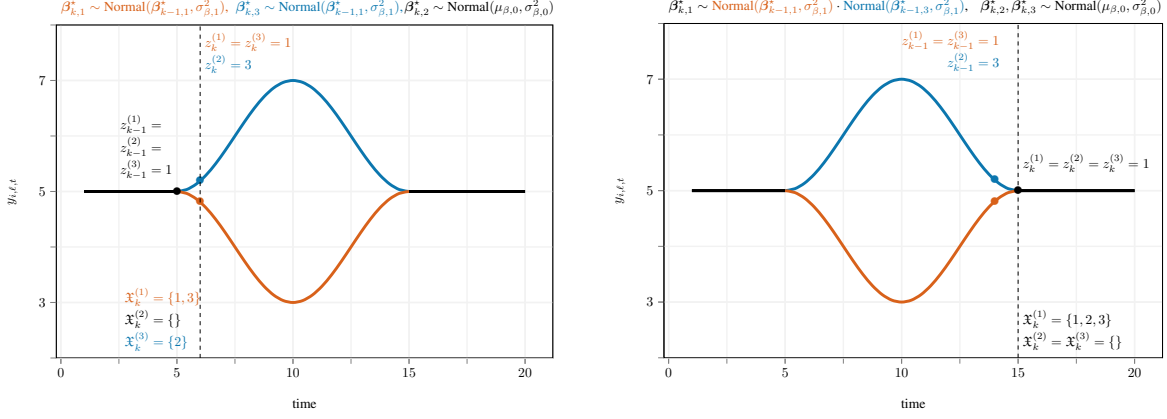


Figure 5: An illustration of the prior on the spline core coefficients  $\beta_{k,z_k}^*$  at location  $k$  (marked by the dashed vertical lines) in the fixed effects model developed in Section 3.1 for a scenario with  $x \in \{1, 2, 3\}$ , where the curves corresponding to the three levels of  $x$  are initially equal, the curves for  $x = 1, 3$  (in blue) and  $x = 2$  (in green) then diverge at  $t = 5$ , merging back again at  $t = 15$ .

quentially as

$$\beta_{k,z_k}^* \sim \begin{cases} \prod_{\{z_{k-1}^{(x)} : x \in \mathfrak{X}_k^{(z_k)}\}} \text{Normal}\left(\beta_{k-1,z_{k-1}^{(x)}}^*, \sigma_{\beta,1}^2\right) & \text{if } |\mathfrak{X}_k^{(z_k)}| > 0, \\ \text{Normal}(\mu_{\beta,0}, \sigma_{\beta,0}^2) & \text{otherwise,} \end{cases} \quad (4)$$

where  $\mathfrak{X}_k^{(z_k)} = \{x : z_k^{(x)} = z_k\}$  is the set of levels of  $x$  that, at the location  $k$ , are assigned the label  $z_k$ . In constructing the prior in this manner, we center the core coefficients around the ones that are ‘expressed’ at the previous location (Figure 5), penalizing their first order differences. The coefficients that are not associated with any levels of  $x$  are assigned a normal prior with a large variance  $\sigma_{\beta,0}^2$ . The initial coefficients are assigned non-informative flat priors as  $\beta_{1,z_k}^* \sim 1$ . The smoothness of the curves is thus controlled by the parameter  $\sigma_{\beta,1}^2$  and is assigned a prior, allowing it to be informed by the data. We let

$$\sigma_{\beta,1} \sim C^+(0, 1),$$

where  $C^+(a, b)$  denotes a half Cauchy distribution (Gelman, 2006; Polson and Scott, 2012) with location parameter  $a$  and scale parameter  $b$ .

### 3.2 Locally Varying Random Effects

We model the time-varying random effects components  $u_i(t)$  as

$$\begin{aligned} u_i(t) &= \sum_{k=1}^K \beta_{k,u,i} b_k(t), \\ \boldsymbol{\beta}_{u,i} &\sim \text{MVN}_K\{\mathbf{0}, (\sigma_{u,a}^{-2} \mathbf{I}_K + \sigma_{u,s}^{-2} \mathbf{P}_u)^{-1}\}, \end{aligned} \quad (5)$$

where  $\boldsymbol{\beta}_{u,i} = (\beta_{1,u,i}, \dots, \beta_{K,u,i})^T$  are subject-specific spline coefficients,  $\text{MVN}_K(\boldsymbol{\mu}, \boldsymbol{\Sigma})$  denotes a  $K$  dimensional multivariate normal distribution with mean  $\boldsymbol{\mu}$  and covariance  $\boldsymbol{\Sigma}$ . We choose  $\mathbf{P}_u = \mathbf{D}_u^T \mathbf{D}_u$ , where the  $(K-1) \times K$  matrix  $\mathbf{D}_u$  is such that  $\mathbf{D}_u \boldsymbol{\beta}_{u,i}$  computes the first order differences in  $\boldsymbol{\beta}_{u,i}$ . The model thus penalizes  $\sum_{k=1}^K (\nabla \beta_{u,i})^2 = \boldsymbol{\beta}_{u,i}^T \mathbf{P}_u \boldsymbol{\beta}_{u,i}$ , the sum of squares of first order differences in  $\boldsymbol{\beta}_{u,i}$  (Eilers and Marx, 1996). The random effects variance parameter  $\sigma_{u,s}^2$  models the smoothness of the random effects curves, smaller  $\sigma_{u,s}^2$  inducing smoother  $u_i(t)$ 's. Additional variations from the constant zero curve are explained by  $\sigma_{u,a}^2$  (Figure 6). The absence of random effects is signified by the limiting case  $\sigma_{u,s}^2 = \sigma_{u,a}^2 = 0$ . We assign half Cauchy priors on the variance parameters as

$$\sigma_{u,s}^2 \sim C^+(0, 1), \quad \sigma_{u,a}^2 \sim C^+(0, 1).$$

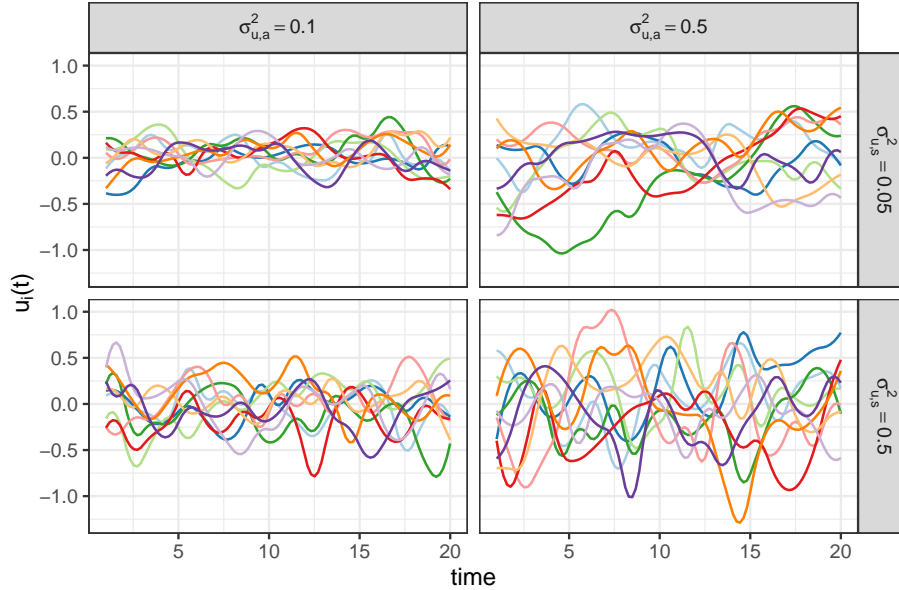


Figure 6: An illustration of the functional random effects model proposed in Section 3.2. Each panel shows a collection of 10 random draws from the random effects distribution for a combination of values of  $(\sigma_{u,s}^2, \sigma_{u,a}^2)$ .

Modeled in the same space of quadratic B-splines, the fixed and the random effects curves thus share similar smoothness properties. Having different smoothness controlling parameters, they are, however, allowed to have different smoothness levels. A similar approach, but with additional assumptions on the covariance matrix of the random effects, has previously been developed in Guo (2002). To our knowledge, model (5) for the random effects is thus also novel.

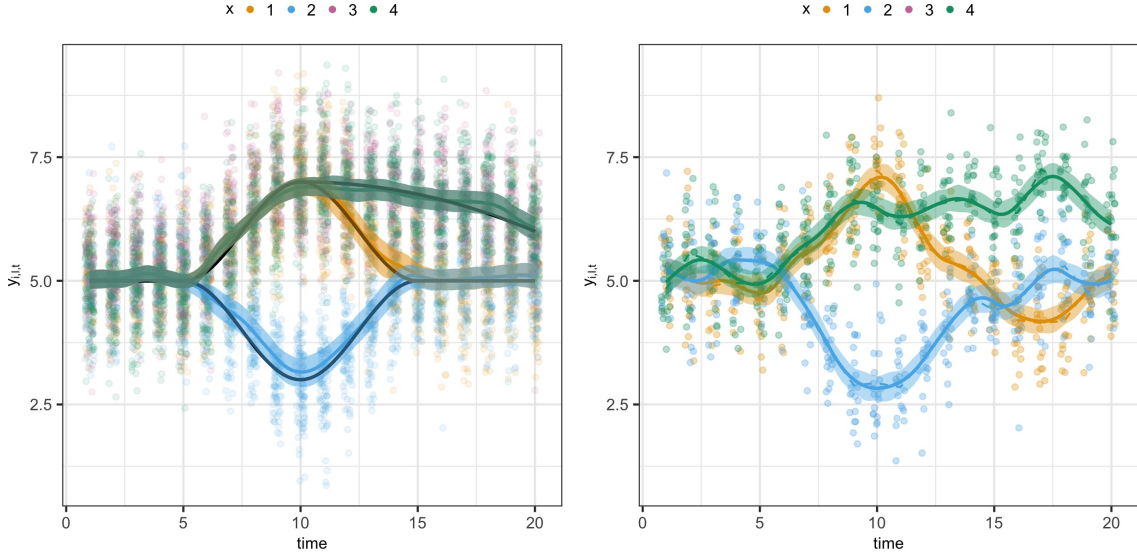


Figure 7: Synthetic example illustrating the performance of the longitudinal mixed model framework developed in Section 3. The left panel shows the true (solid black lines) fixed effects curves, and their estimated posterior means and point wise 90% credible intervals, superimposed on slightly jittered response values  $y_{i,\ell,t}$  for different levels of  $x$ . The right panel shows three examples of true (dashed lines) individual specific curves, their estimated posterior means (solid lines) and 90% point wise credible intervals, superimposed on the associated jittered response values  $y_{i,\ell,t}$ .

### 3.3 Illustrative Example

An example helps illustrate the workings of the proposed longitudinal mixed model framework. Figure 7 depicts a synthetic scenario with  $x \in \{1, 2, 3, 4\}$  and a Gaussian likelihood function  $f_y\{y_{i,\ell,t} \mid \theta_x^{(i)}(t), \theta_\epsilon\} = \text{Normal}\{\theta_x^{(i)}(t), \sigma_\epsilon^2\}$ . The true fixed effects curves corresponding to the four levels of  $x$  start equal at  $t = 0$ , then the effect of level 2 diverges from that of 1, 3, 4 at  $t = 5$ , the effect of levels 3, 4 further diverges from that of 1 at  $t = 10$ , the effects of the levels 1 and 2 then merge back at  $t = 15$ , but the effect of levels 3, 4 continues to remain different until the end  $t = 20$ . In each case, we simulated  $n = 20$  individuals with  $L = 10$  number of trials. Our proposed method has done an excellent job of estimating the underlying true population and individual level curves and their local dependency structures (Figure 7).

This concludes the description of the novel generic longitudinal mixed model framework. A rigorous study of its statistical properties is being pursued as the subject of a separate manuscript (Paulon and Sarkar, 2020). In the following section, we focus on adapting this framework to develop a novel longitudinal drift-diffusion mixed model for our motivating tone learning and decision making problem.

## 4 Longitudinal Drift-Diffusion Mixed Models

The basic Wiener diffusion process can be specified as  $W(\tau) = \mu\tau + \sigma B(\tau)$ , where  $B(\tau)$  is the standard Brownian motion,  $\mu$  is the drift rate, and  $\sigma$  is the diffusion coefficient (Cox and Miller, 1965; Ross *et al.*, 1996). The process has independent normally distributed increments, that is,  $\Delta W(\tau) = \{W(\tau + \Delta\tau) - W(\tau)\} \sim \text{Normal}(\mu\Delta\tau, \sigma^2\Delta\tau)$ , independently from  $W(\tau)$ . The first passage time of crossing a threshold  $b$ ,  $\tau = \inf\{\tau' : W(0) = 0, W(\tau') \geq b\}$ , is then distributed according to an inverse Gaussian distribution (Whitmore and Seshadri, 1987; Chhikara, 1988; Lu, 1995) with density

$$f(\tau \mid \mu, \sigma^2, b) = \frac{b}{\sqrt{2\pi\sigma^2}} \tau^{-3/2} \exp\left\{-\frac{(b-\mu\tau)^2}{2\sigma^2\tau}\right\}, \quad b > 0, \quad \mu > 0, \quad \sigma^2 > 0.$$

With  $\boldsymbol{\theta} = (\mu, \sigma, b)^T$ , we have  $\mathbb{E}(\tau \mid \boldsymbol{\theta}) = b/\mu$  and  $\text{var}(\tau \mid \boldsymbol{\theta}) = b\sigma^2/\mu^3$ .

Given a perceptual stimuli and a set of decision choices, the neurons in the brain accumulate evidence in favor of the different alternatives. Modeling this behavior using Wiener processes with unit variances, assuming that a response is initiated when the decision threshold for one of the options is crossed, a probability model for the time  $\tau_d$  to reach the threshold for the  $d^{th}$  decision category under the influence of the  $s^{th}$  stimulus is obtained as

$$f(\tau_d \mid \delta_s, \mu_{d,s}, 1, b_{d,s}) = \frac{b_{d,s}}{\sqrt{2\pi}} (\tau_d - \delta_s)^{-3/2} \exp\left[-\frac{\{b_{d,s} - \mu_{d,s}(\tau_d - \delta_s)\}^2}{2(\tau_d - \delta_s)}\right], \quad (6)$$

where  $\mu_{d,s}$  denotes the rate of accumulation of evidence,  $b_{d,s}$  the decision boundaries, and  $\delta_s$  an offset representing the time required to encode the  $s^{th}$  signal before evidence accumulation begins (Figure 2). We now let  $\boldsymbol{\theta}_{d,s} = (\delta_s, \mu_{d,s}, b_{d,s})^T$ . Since a decision  $d$  is reached at response time  $\tau$  if the corresponding threshold is crossed first, that is when  $\{\tau = \tau_d\} \cap_{d' \neq d} \{\tau_{d'} > \tau_d\}$ , we have  $y = \arg \min \tau_{d'}$ . Assuming simultaneous accumulation of evidence for all decision categories, modeled by independent Wiener processes, and termination when the threshold for the observed decision category  $d$  is reached, the joint distribution of  $(d, \tau)$  is thus given by

$$f(d, \tau \mid s, \boldsymbol{\theta}) = g(\tau \mid \boldsymbol{\theta}_{d,s}) \prod_{d' \neq d} \{1 - G(\tau \mid \boldsymbol{\theta}_{d',s})\}. \quad (7)$$

where, to distinguish from the generic notation  $f$ , we now use  $g(\cdot \mid \boldsymbol{\theta})$  and  $G(\cdot \mid \boldsymbol{\theta})$  to denote, respectively, the probability density function (pdf) and the cumulative distribution function (cdf) of an inverse-Gaussian distribution, as defined in (6). The marginal probability of taking decision  $d$  under the influence of stimulus  $s$  is then obtained as

$$P(d \mid s) = \int_{\delta_s}^{\infty} g(\tau \mid \boldsymbol{\theta}_{d,s}) \prod_{d' \neq d} \{1 - G(\tau \mid \boldsymbol{\theta}_{d',s})\} d\tau. \quad (8)$$

Interestingly, model (8) is similar to traditional multinomial probit/logit regression models (Borooah, 2002; Agresti, 2018) except that the latent variables are now inverse-Gaussian distributed as opposed to being normal or extreme-value distributed, and the observed category is associated with the minimum of the latent variables in contrast to being identified with the maximum of the latent variables. We thus refer to model (7) and (8) as an inverse-Gaussian drift-diffusion model and a multinomial inverse-probit model, respectively. To the best of our knowledge, models (7)-(8) themselves are novel to the literature.

For the longitudinal tone categorization experiment described in Section 2, let  $s_{i,\ell,t}$  denote the input tone for the  $i^{\text{th}}$  individual in the  $\ell^{\text{th}}$  trial on day  $t$ . Likewise, let  $d_{i,\ell,t}$  and  $\tau_{i,\ell,t}$  denote, respectively, the selected Mandarin tone and the time taken to reach the corresponding threshold by the  $i^{\text{th}}$  individual in the  $\ell^{\text{th}}$  trial on day  $t$ . We now have

$$f\{\tau_{i,\ell,t} \mid s_{i,\ell,t} = s, \boldsymbol{\theta}_{d,s}^{(i)}(t)\} = \frac{b_{d,s}^{(i)}(t)}{\sqrt{2\pi}(\tau_{i,\ell,t} - \delta_s)^{3/2}} \exp \left[ -\frac{\{b_{d,s}^{(i)}(t) - \mu_{d,s}^{(i)}(t)(\tau_{i,\ell,t} - \delta_s)\}^2}{2(\tau_{i,\ell,t} - \delta_s)} \right]. \quad (9)$$

The drift rates  $\mu_{d,s}^{(i)}(t)$  and the decision boundaries  $b_{d,s}^{(i)}(t)$  now also vary with time  $t$ . In addition, we accommodate random effects by allowing  $\mu_{d,s}^{(i)}(t)$  and  $b_{d,s}^{(i)}(t)$  to also depend on the subject index  $i$ . Letting  $y_{i,\ell,t} = (d_{i,\ell,t}, \tau_{i,\ell,t})$ , the likelihood function of our longitudinal drift-diffusion mixed model thus takes the form

$$L(\mathbf{y} \mid \mathbf{s}, \boldsymbol{\theta}) = \prod_{d=1}^{d_0} \prod_{t=1}^T \prod_{i=1}^n \prod_{\ell=1}^{m_{i,t}} \left( g\{\tau_{i,\ell,t} \mid \boldsymbol{\theta}_{d,s}^{(i)}(t)\} \prod_{d' \neq d} [1 - G\{\tau_{i,\ell,t} \mid \boldsymbol{\theta}_{d',s}^{(i)}(t)\}] \right)^{1_{\{d_{i,\ell,t}=d\}}}.$$

We model the longitudinal mixed effects parameters  $\mu_{d,s}^{(i)}(t)$ ,  $b_{d,s}^{(i)}(t)$  using the framework developed in Section 3. Following the notation of Section 3, the categorical variable indexing the parameters is thus  $x = (d, s) \in \mathcal{X} = \{(1, 1), (1, 2), \dots, (4, 4)\}$ . We also need an additional exponentiation step to enforce positivity conditions. For any participant, the random effects for correct and incorrect identification of the tones are generally expected to be different and on the opposite sides of the corresponding population level curves. We thus allow different random effects  $u^{(C,i)}(t)$  and  $u^{(I,i)}(t)$

for correct (C) and incorrect (I) identifications, respectively. The model for the drift rates  $\mu_x^{(i)}(t)$  is thus specified as

$$\begin{aligned} \mu_x^{(i)}(t) &= \exp\{f_{\mu,x}(t) + u_{\mu}^{(C,i)}(t)\} \quad \text{when } d = s, \\ \mu_x^{(i)}(t) &= \exp\{f_{\mu,x}(t) + u_{\mu}^{(I,i)}(t)\} \quad \text{when } d \neq s, \\ \{f_{\mu,x}(t) \mid z_k^{(x)} = z_k\} &= \sum_{k=1}^K \beta_{\mu,k,z_k}^* b_k(t), \\ u_{\mu}^{(i)}(t) &= \sum_{k=1}^K \beta_{\mu,k,u}^{(i)} b_k(t), \quad \beta_{\mu,u}^{(i)} \sim \text{MVN}_K\{\mathbf{0}, (\sigma_{\mu,u,a}^{-2} \mathbf{I}_K + \sigma_{\mu,u,s}^{-2} \mathbf{P}_u)^{-1}\}, \end{aligned}$$

where, at the parameter levels, we define  $u_{\mu}^{(i)}(t)$  to be the normally distributed time varying random effects. Integrating out the random effects, the corresponding population level model  $\mu_x(t)$  is obtained as

$$\mu_x(t) = \int \exp\{f_{\mu,x}(t) + u_{\mu}^{(i)}(t)\} f\{u_{\mu}^{(i)}(t)\} du_{\mu}^{(i)}(t) = \exp\left[f_{\mu,x}(t) + \frac{\text{var}\{u_{\mu}^{(i)}(t)\}}{2}\right].$$

Individual and population level models for the boundaries  $b_x^{(i)}(t)$  are specified likewise. The latent cluster inducing variable  $z_k^{(x)}$  is shared between the models for  $\mu_x^{(i)}(t)$  and  $b_x^{(i)}(t)$ , facilitating model interpretability. We assign uniform priors on  $\delta_s \sim \text{Unif}(0, \delta_{s,\max})$ , where  $\delta_{s,\max}$  is the minimum of all response times under stimulus  $s$ , that is,  $\delta_{s,\max} = \min_{\{(i,\ell,t): s_{i,\ell,t}=s\}} \tau_{i,\ell,t}$ .

We consider two types of dynamics for the latent states corresponding to correct (C) and incorrect (I) identification of the tones. That is, we let

$$\begin{aligned} (z_k^{(d,s)} \mid z_{k-1}^{(d,s)} = z_{k-1}) &\sim \text{Mult}(\pi_{z_{k-1},1}^{(C)}, \dots, \pi_{z_{k-1},z_{\max}}^{(C)}) \quad \text{when } d = s, \\ (z_k^{(d,s)} \mid z_{k-1}^{(d,s)} = z_{k-1}) &\sim \text{Mult}(\pi_{z_{k-1},1}^{(I)}, \dots, \pi_{z_{k-1},z_{\max}}^{(I)}) \quad \text{when } d \neq s. \end{aligned}$$

We assign hierarchical Dirichlet priors on the transition probabilities

$$\boldsymbol{\pi}_z^{(C)} = (\pi_{z,1}^{(C)}, \dots, \pi_{z,z_{\max}}^{(C)})^T \sim \text{Dir}(\alpha^{(C)}/z_{\max}, \dots, \alpha^{(C)}/z_{\max}) \quad \text{with} \quad \alpha^{(C)} \sim \text{Ga}(a, b).$$

and an analogous expression holds for  $\boldsymbol{\pi}_z^{(I)}$  and  $\alpha^{(I)}$ .

Importantly, although the different values of  $x = (d, s)$  create a natural partition of the data set just like the framework in Section 3, unlike before, for any decision  $d$  produced under the input tone  $s$ , all four latent variables  $z_k^{(1,s)}, z_k^{(2,s)}, z_k^{(3,s)}, z_k^{(4,s)}$  now simultaneously appear in the likelihood function (7). The graphical model (Figure 8 and Figure S.5 in the supplementary materials) thus resembles a factorial HMM (Ghahramani and Jordan, 1997, fHMM). Given the data, a latent state  $z_k^{(d,s)}$  is now informed by all responses generated under the tone  $s$ , not just the subset corresponding to  $x = (d, s)$ . This has important consequences for posterior inference, as we



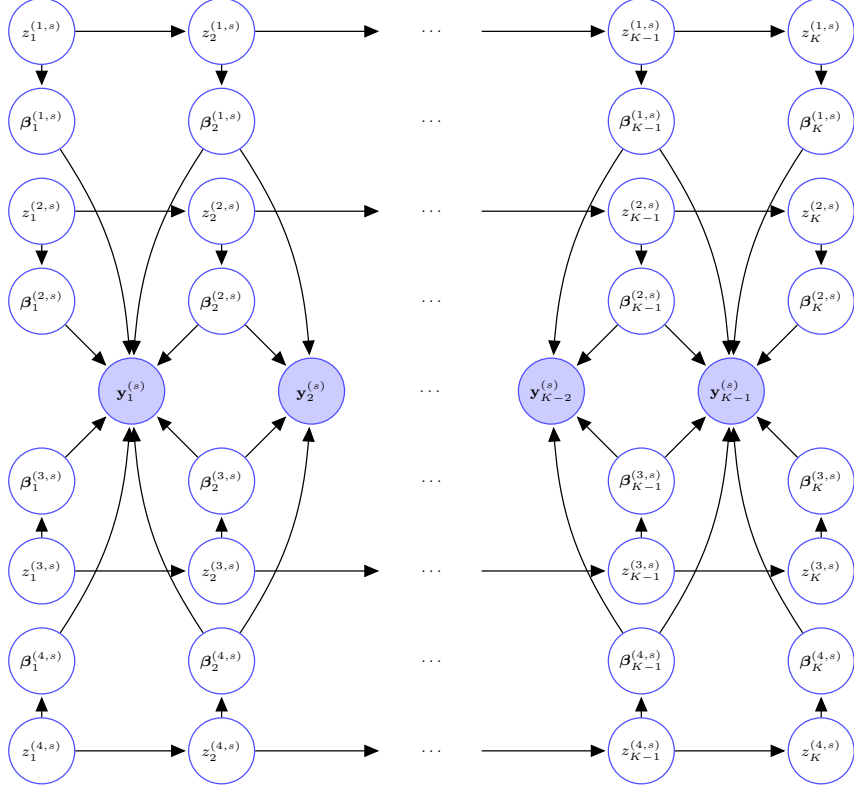


Figure 8: Graph of the proposed model for tone learning.

discuss below.

## 5 Posterior Inference

In simpler likelihood settings, posterior inference for the longitudinal mixed model framework developed in Section 3 can generally be based on samples drawn from the posterior using dynamic message passing MCMC algorithms (Rabiner, 1989; Scott, 2002) that carefully exploits the conditional independence relationships encoded in the model. In this article, we focus on computational strategies for the drift-diffusion mixed model adaptation, in which case, the nonstandard inverse-Gaussian likelihood and the fHMM type model structure bring in significant additional complexities. We adapt recent advances in MCMC algorithms for discrete spaces (Neal, 2003; Van Gael *et al.*, 2008; Titsias and Yau, 2014; Zanella, 2019) in novel non-trivial ways, designing locally informative slice sampling moves that overcome these challenges. Due to space constraints, the details are deferred to Section S.5 in the supplementary materials.

## 6 Application to Tone Categorization Data

In this section, we discuss the results produced by our method applied to the tone category learning data described in Section 2. Our primary inference goals, we recall, include understanding systematic longitudinal variations in perceptual categorization decision as the participants get better at identifying the tones with there being some additional interests in assessing individual specific trajectories, especially how they differ between fast and slow learners.

Figure 9 shows the posterior mean trajectories and associated 90% credible intervals for the boundaries  $b_{d,s}(t)$  and the drift rates  $\mu_{d,s}(t)$  estimated by our method for different combinations of  $(d, s)$ . Figure 10 reports the probabilities of each of the  $\binom{4}{2} = 6$  pairs of success ( $d = s$ ) parameters to cluster together in different blocks. These results suggest that after an initial learning phase where the underlying processes are all similar across all input tones, there are two main learning groups. Tones {T1, T3} seem to be easier to learn, as the corresponding drift parameters are larger, and tones {T2, T4} are more challenging. After the fifth block, however, the groups become {T3} and {T1, T2, T4}. In this phase, tone T3 thus seems easier to distinguish from others as its drift parameter is larger. These findings are confirmed by empirical summaries of the data. In fact, the similarity groups of the mandarin tones are {T1, T3}, which are characterized by the height of the pitch, and tones {T2, T4}, which are characterized by the direction of the pitch and are more challenging to learn. Tone T3, in particular, is special because it has no equivalent in the English language and therefore is easier to categorize (Song *et al.*, 2008). Our proposed method allows similar inferential questions to be answered for the drift parameters corresponding to misclassifications, as well as for all the boundary parameters. The misclassification drift curves are mostly similar to each other, although some minor local differences can be found. Notable exceptions are  $\mu_{1,3}(t)$  and  $\mu_{3,1}(t)$  which are significantly smaller than all other drifts after the third block. As the participants get trained and experienced, for input tone T1, evidence in favor of tone T3 is thus collected more slowly compared to evidence in favor of T2 and T4, and vice versa. Likewise, while the boundary curve estimates mostly remain constant over time and similar to each other,  $b_{1,3}(t)$  and  $b_{3,1}(t)$  again differ from the rest and actually increase over time. As the participants get trained and experienced, more evidence in favor of tone T3 is thus needed to misclassify tone T1 as tone T3 and vice versa. These suggest that, as the participants get trained and experienced, tones T1 and T3 become harder to misclassify for one another.

Importantly, our proposed drift-diffusion mixed model not only allows population level inference about the underlying processes but also allows us to efficiently estimate individual specific parameter trajectories. Figure 11 shows the posterior mean trajectories and associated 90% credible intervals for the drift rates  $\mu_{s,d}^{(i)}$  and the boundaries  $b_{s,d}^{(i)}$  estimated by our method for the different success combinations of  $(d, s)$  for two

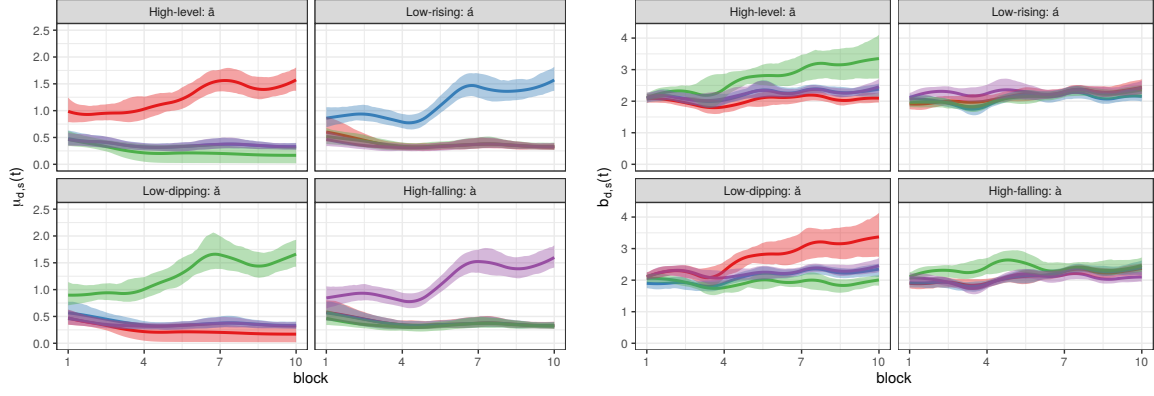


Figure 9: Results for tone learning data: Estimated posterior mean trajectories of the population level drifts  $\mu_{d,s}(t)$  (left panel) and boundaries  $b_{d,s}(t)$  (right panel) for the proposed longitudinal inverse-Gaussian drift-diffusion mixed model. The shaded areas represent corresponding 90% point wise credible intervals. Parameters for the high-flat tone response category T1 are shown in red; low-rising T2 in blue; low-dipping T3 in green; and high-falling T4 in purple.

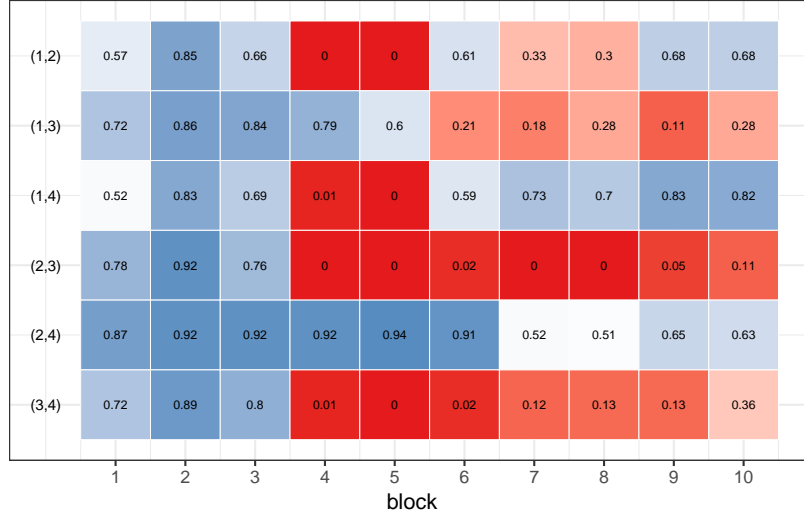


Figure 10: Results for tone learning data: Pairwise posterior co-clustering probabilities of underlying parameter trajectories for successful identification ( $d = s$ ) of different input tones in different learning phases. The estimated posterior probability of  $(\mu_{2,2}, b_{2,2})$  and  $(\mu_{3,3}, b_{3,3})$  being clustered together, and hence being equal, in the 6<sup>th</sup> block is thus 0.02, as shown in row (2,3) and column 6. Equivalently, the estimated posterior probability of  $(\mu_{2,2}, b_{2,2})$  and  $(\mu_{3,3}, b_{3,3})$  being different in the 6<sup>th</sup> block is 0.98.

participants - the one with the best accuracy averaged across all blocks, and the one with the worst accuracy averaged across all blocks. These show that the individual level drift and boundary trajectories can be significantly different from the corresponding population level estimates. The differences in the performances can again

be explained mostly by differences in the drift trajectories. For the well performing participant, the drift trajectories increase rapidly with time before plateauing down around block 6, at which stage the participant has already attained native-like proficiency. For the poorly performing candidate on the other hand, the drift trajectories remain approximately constant across all 10 blocks.

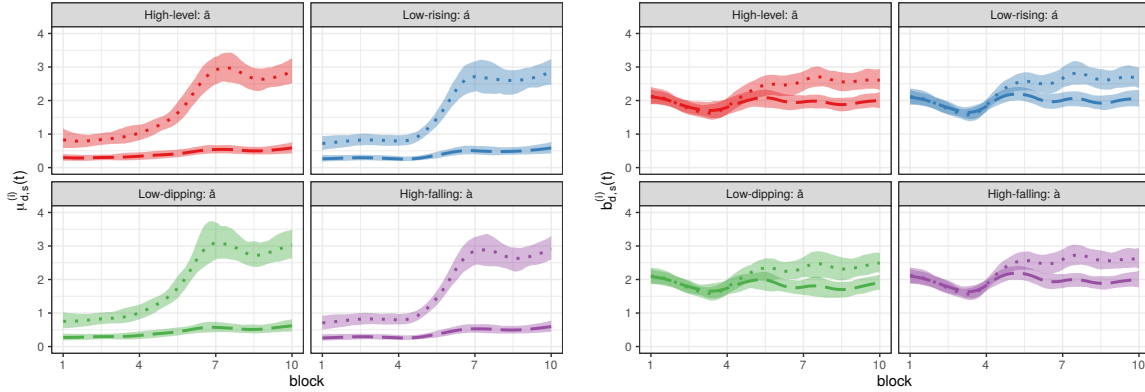


Figure 11: Results for tone learning data: Estimated posterior mean trajectories for individual specific drifts  $\mu_{d,s}^{(i)}(t)$  (left panel) and boundaries  $b_{d,s}^{(i)}(t)$  (right panel) for successful identification ( $d = s$ ) for two different participants - one performing well (dotted line) and one performing poorly (dashed line). The shaded areas represent corresponding 90% point wise credible intervals. Parameters for the high-flat tone response category T1 are shown in red; low-rising T2 in blue; low-dipping T3 in green; and high-falling T4 in purple.

We compare the performance of our method with that of the linear ballistic accumulator (LBA) model (Brown and Heathcote, 2008). Similar to our model, the LBA uses independent evidence accumulators starting at  $\delta_s$  that continue until a response threshold  $b_s$  is reached. The accumulator that first reaches the boundary corresponds to the decision outcome, and the time taken to reach this decision boundary is the observed response time. The LBA model, however, assumes that the evidence accumulates linearly at the rate  $\mu$ , reaching the boundary  $b$  precisely at time  $\tau = b/\mu$ . Unlike in drift-diffusion models, where trial-by-trial variability is explained by stochastically different diffusion paths, the LBA model explains trial-by-trial variability assuming the slopes  $\mu$  for different trials to be drawn from a  $\text{Normal}(m_{d,s}, v_{d,s})$  distribution. (Figure S.6 in the supplementary materials).

The literature on LBA models has many serious limitations. The normality assumption on the slopes  $\mu$  clearly does not satisfy any non-negativity constraints. Existing LBA models are also limited in their use of a common boundary  $b_s$  for all input stimuli  $s$ . There is also no principled way to incorporate systematic stimulus and decision category specific fixed or individual specific random effects into the LBA model. Existing literature is also limited to static settings, there is no mechanism to estimate smoothly varying longitudinal parameter trajectories as the participants get

trained and experienced in their decision tasks. In our implementation, we thus fitted the LBA model separately for each block. Finally, the likelihood function of the LBA model is non-convex in the parameters. Parameter estimation based on optimization of the likelihood function is thus fraught with convergence issues. We used the `rtdists` package (Singmann *et al.*, 2019) in R, using several random initializations and tracking the objective function to ensure convergence. A more detailed review of the LBA model can be found in Section S.6 of the supplementary materials.

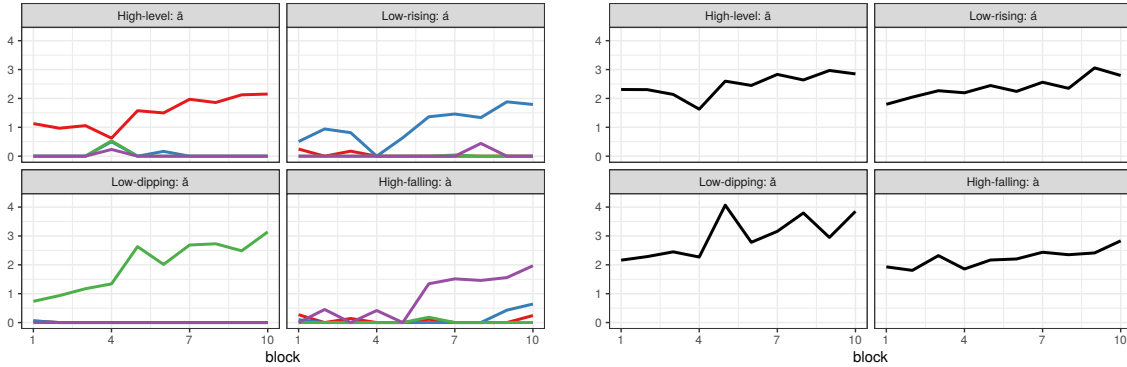


Figure 12: Results for tone learning data: Left: estimated mean slopes  $m_{d,s,t}$  for the LBA model. Right: estimated boundaries  $b_{s,t}$  for the LBA model. In the left panel,  $m_{d,s,t}$ 's for the high-flat tone response category T1 are shown in red; low-rising T2 in blue; low-dipping T3 in green; and high-falling T4 in purple.

Results produced by the LBA model applied to our motivating tone-learning data are reported in Figure 12. Owing to the limitations discussed above, the inference we can do with such models is very limited. For instance, only non-smooth population level estimates are available, individual specific trajectories can not be assessed, etc. Some of our findings can, however, be confirmed by the LBA method. For example, looking at the drift parameter estimates, one can see that tone T3 is consistently associated with larger drifts. As was also seen in the estimates returned by our method, tones {T2, T4} have similar values for the drift and the boundary parameters. Except such general overall findings, the LBA model, however, can not answer scientific questions related to the dynamics of category learning with fine detail.

Our method, on the other hand, provides a biologically interpretable yet statistically principled approach to accommodate fixed effects of input stimuli and decision categories as well as random subject specific heterogeneity, allows MCMC algorithm based efficient estimation of longitudinally smoothly evolving parameter trajectories, borrowing information across population subgroups, participants as well as adjacent time stamps through many layers of hierarchy. Crucially, building on the local cluster inducing model of Section 3, our method also allows automated assessment of local similarities and differences in the parameter trajectories in very fine detail as the participants get trained and experienced in their decision tasks.

## 7 Simulation Studies

In this section, we discuss the results of synthetic experiments related specifically to drift-diffusion models. We are not aware of any other method in the existing literature that can be readily applied or at least be easily adapted to our data settings and inferential challenges. We thus also restrict our focus on evaluating the performance of the proposed longitudinal inverse-Gaussian drift-diffusion mixed model only.

In designing the simulation scenarios, we have tried to closely mimic our motivating tone learning data set. We thus chose  $n = 20$  participants being trained over  $T = 10$  blocks to identify  $d_0 = 4$  tones. We set  $\mu_{d,s}(t), b_{d,s}(t)$  to values that are very similar to the corresponding estimated values for the real data set. As in the real data set, the local differences were all set to be in the drift curves; additionally, some boundary trajectories were globally different from each other. We slightly simplified the local clustering structure, however, to be able to better illustrate the workings of our proposed method. Moreover, we choose  $u_\mu^{(C,i)}(t), u_b^{(C,i)}(t), u_\mu^{(I,i)}(t), u_b^{(I,i)}(t), \delta_s$  etc. to be the estimated posterior means obtained for the real data set.

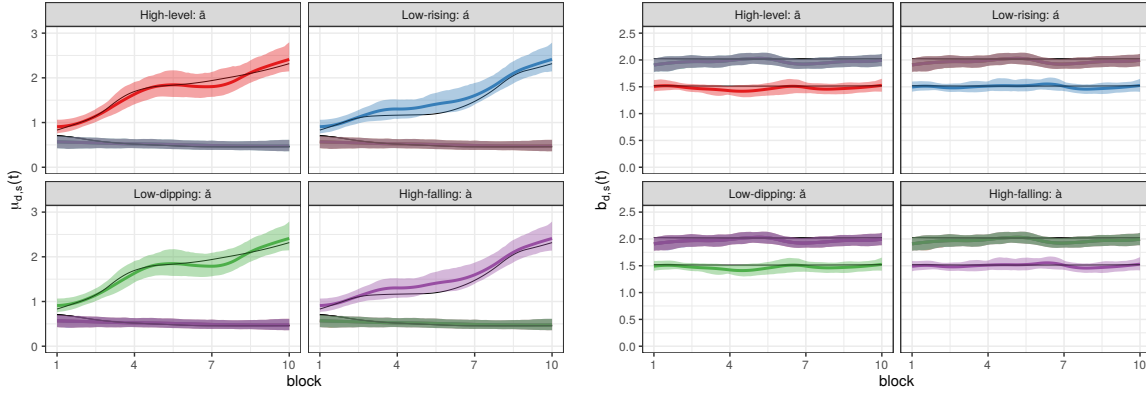


Figure 13: Results for synthetic data: Estimated posterior mean trajectories of the population level drifts  $\mu_{d,s}(t)$  (left panel) and boundaries  $b_{d,s}(t)$  (right panel) for the proposed longitudinal inverse-Gaussian drift-diffusion mixed model. The shaded areas represent corresponding 90% point wise credible intervals. The solid black lines represent underlying true curves. Parameters for the high-flat tone response category T1 are shown in red; low-rising T2 in blue; low-dipping T3 in green; and high-falling T4 in purple.

Figure 13 shows the posterior mean trajectories and associated 90% credible intervals for the drift rates  $\mu_{d,s}(t)$  and boundaries  $b_{d,s}(t)$ , for every possible combination of  $(d, s)$ . Figure S.10 in the supplementary materials additionally presents the drift curves for successful identifications ( $d = s$ ) superimposed on each other. These figures suggest that the underlying true curves are all recovered well by our method. In comparison, the results obtained by the LBA model, displayed in Figure 14, suffer from the same limitations discussed in Section 6. Furthermore, Figures S.8 and S.9

in supplementary materials suggest that the underlying true local partition structure, as well as the individual specific parameter trajectories, are also estimated extremely well by our method.

Figure 14 presents the results obtained by the LBA model applied to the synthetic data set. There is a general agreement between the population level estimates produced by our method and the LBA. However, as discussed in detail in Section 6 in the main paper and Section S.6 in the supplementary materials, the LBA model has many serious limitations, including being incapable of producing individual level estimates, having shared boundary parameters across all input tones, not borrowing any information across adjacent time stamps etc. Only a very limited set of inferential questions can therefore be answered by the LBA model.

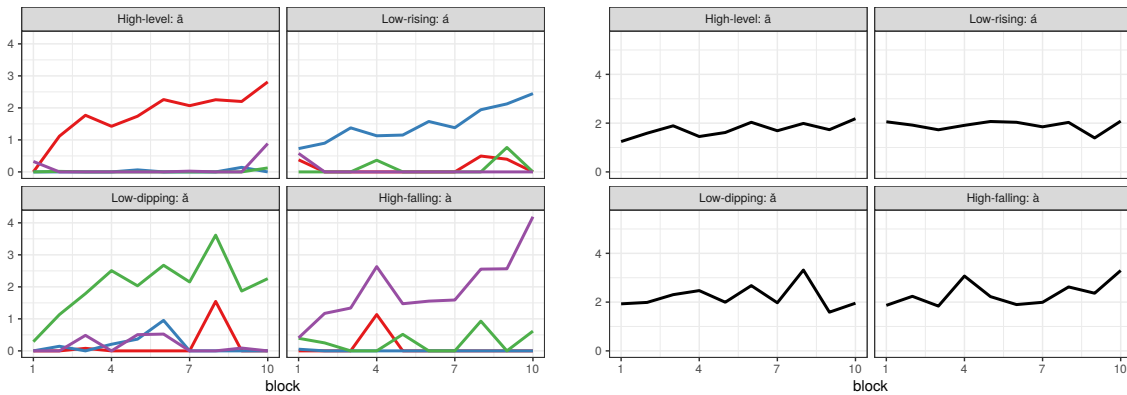


Figure 14: Results for synthetic data: Left: estimated mean slopes  $m_{d,s,t}$  for the LBA model. Right: estimated boundaries  $b_{s,t}$  for the LBA model. In the left panel,  $m_{d,s,t}$ 's for the high-flat tone response category T1 are shown in red; low-rising T2 in blue; low-dipping T3 in green; and high-falling T4 in purple.

## 8 Discussion

**Summary:** In this article, we proposed a novel longitudinal drift-diffusion mixed model for perceptual decision making, allowing the underlying mechanisms to be similar or different at different longitudinal stages. Our research was motivated primarily by auditory neuroscience experiments where scientists are interested in understanding how the decision making mechanisms evolve as the participants get more training in the decision tasks. Our model was built on a novel statistical framework for longitudinal data that exploited local support properties of B-spline bases and (factorial) HMMs to allow automated assessment of local similarities and differences in the underlying parameter trajectories.

Application to our motivating tone categorization experiments provided interesting novel insights into the underlying learning mechanisms. Notably, we discovered

that the improvements in the performance and the local variations can be explained mostly due to local variations in the underlying drift parameters. We also discovered local groupings among the underlying parameter curves in various phases of the learning experiments, how they differ between well and poorly performing participants etc. Such inferences are completely outside the scope of the previously existing literature.

**Broader statistics impact:** The flexible longitudinal framework proposed in this article is generic in nature with applications not limited to drift-diffusion models but can be easily adapted to a broad variety of other likelihood models. A major component of our ongoing research and the subject of multiple separate manuscripts focuses on adapting the proposed framework to diverse other statistical models, including other models directly relevant to auditory neuroscience research.

**Broader scientific impact:** The proposed approach, we believe, also takes the existing literature on drift-diffusion decision making models many significant steps forward, enabling neuroscientists to study the longitudinal behavior of the biologically interpretable model parameters in much finer detail than what previous methods could achieve. As reported in Section 6, the findings in our motivating speech learning experiment are also scientifically highly significant. Efficient estimation of individual level trajectories open exciting avenues for potential adaptations in clinical settings. See also Section S.1 in the supplementary materials. Importantly, the scope of proposed method is also not restricted to auditory neuroscience problems but the approach can be readily applied to study decision making mechanisms in other areas of neuroscience as well.

## Supplementary Materials

The supplementary materials present brief reviews of current neurobiological models of speech learning, fHMMs, B-splines, locally informed Hamming ball samplers, the linear ballistic accumulator model etc. for easy reference. The supplementary materials also detail the choice of hyper-parameters and the MCMC algorithm used to sample from the posterior. The supplementary materials additionally include the tone categorization data set described in Section 2 and analyzed in Section 6, and R programs implementing the longitudinal drift-diffusion mixed model developed in this article.

## Acknowledgments

This work was supported by the National Institute on Deafness and Other Communication Disorders grants R01DC013315 and R01DC015504, awarded to Chandrasekaran.



## References

- Agresti, A. (2018). *An introduction to categorical data analysis*. Wiley.
- Bogacz, R., Wagenmakers, E.-J., Forstmann, B. U., and Nieuwenhuis, S. (2010). The neural basis of the speed-accuracy tradeoff. *Trends in Neurosciences*, **33**, 10–16.
- Borooah, V. K. (2002). *Logit and probit: ordered and multinomial models*. Sage.
- Brody, C. D. and Hanks, T. D. (2016). Neural underpinnings of the evidence accumulator. *Current Opinion in Neurobiology*, **37**, 149–157.
- Brown, S. D. and Heathcote, A. (2008). The simplest complete model of choice response time: Linear ballistic accumulation. *Cognitive Psychology*, **57**, 153–178.
- Cappé, O., Moulines, E., and Rydén, T. (2005). *Inference in hidden Markov models*. Springer Verlag, Berlin.
- Cavanagh, J. F., Wiecki, T. V., Cohen, M. X., Figueroa, C. M., Samanta, J., Sherman, S. J., and Frank, M. J. (2011). Subthalamic nucleus stimulation reverses mediofrontal influence over decision threshold. *Nature Neuroscience*, **14**, 1462.
- Chandrasekaran, B., Sampath, P. D., and Wong, P. C. (2010). Individual variability in cue-weighting and lexical tone learning. *The Journal of the Acoustical Society of America*, **128**, 456–465.
- Chhikara, R. (1988). *The inverse Gaussian distribution: Theory, methodology, and applications*. CRC Press.
- Chib, S. and Hamilton, B. H. (2002). Semiparametric bayes analysis of longitudinal data treatment models. *Journal of Econometrics*, **110**, 67–89.
- Cox, D. R. and Miller, H. D. (1965). *The theory of stochastic processes*. CRC Press.
- Craigmile, P. F., Peruggia, M., and Van Zandt, T. (2010). Hierarchical Bayes models for response time data. *Psychometrika*, **75**, 613–632.
- Daniels, M. J. and Pourahmadi, M. (2002). Bayesian analysis of covariance matrices and dynamic models for longitudinal data. *Biometrika*, **89**, 553–566.
- de Boor, C. (1978). *A practical guide to splines*. Springer-Verlag.
- Diggle, P., Diggle, P. J., Heagerty, P., Heagerty, P. J., Liang, K.-Y., Zeger, S., *et al.* (2002). *Analysis of longitudinal data*. Oxford University Press.
- Ding, L. and Gold, J. I. (2013). The basal ganglia’s contributions to perceptual decision making. *Neuron*, **79**, 640–649.
- Dufau, S., Grainger, J., and Ziegler, J. C. (2012). How to say “no” to a nonword: A leaky competing accumulator model of lexical decision. *Journal of Experimental Psychology: Learning, Memory, and Cognition*, **38**, 1117.

- Eilers, P. H. and Marx, B. D. (1996). Flexible smoothing with b-splines and penalties. *Statistical Science*, **11**, 89–102.
- Feng, G., Yi, H. G., and Chandrasekaran, B. (2018). The role of the human auditory corticostriatal network in speech learning. *Cerebral Cortex*, pages 1–13.
- Fitzmaurice, G., Davidian, M., Verbeke, G., and Molenberghs, G. (2008). *Longitudinal data analysis*. CRC Press.
- Frühwirth-Schnatter, S. (2006). *Finite mixture and Markov switching models*. Springer, New York.
- Gelman, A. (2006). Prior distributions for variance parameters in hierarchical models. *Bayesian Analysis*, **1**, 515–534.
- Ghahramani, Z. and Jordan, M. I. (1997). Factorial hidden Markov models. *Machine Learning*, **29**, 245–273.
- Glimcher, P. W. and Fehr, E. (2013). *Neuroeconomics: Decision making and the brain*. Academic Press.
- Gold, J. I. and Shadlen, M. N. (2007). The neural basis of decision making. *Annual Review of Neuroscience*, **30**, 535–574.
- Guo, W. (2002). Functional mixed effects models. *Biometrics*, **58**, 121–128.
- Heekeren, H. R., Marrett, S., Bandettini, P. A., and Ungerleider, L. G. (2004). A general mechanism for perceptual decision-making in the human brain. *Nature*, **431**, 859.
- Iverson, P., Kuhl, P. K., Akahane-Yamada, R., Diesch, E., Tohkura, Y., Kettermann, A., and Siebert, C. (2003). A perceptual interference account of acquisition difficulties for non-native phonemes. *Cognition*, **87**, 47–57.
- Johnson, J. S. and Newport, E. L. (1989). Critical period effects in second language learning: The influence of maturational state on the acquisition of english as a second language. *Cognitive Psychology*, **21**, 60–99.
- Leite, F. P. and Ratcliff, R. (2010). Modeling reaction time and accuracy of multiple-alternative decisions. *Attention, Perception, & Psychophysics*, **72**, 246–273.
- Li, Y., Lin, X., and Müller, P. (2010). Bayesian inference in semiparametric mixed models for longitudinal data. *Biometrics*, **66**, 70–78.
- Lu, J. (1995). *Degradation processes and related reliability models*. Ph.D. thesis, McGill University, Montreal, Canada.
- Maddox, W. T. and Chandrasekaran, B. (2014). Tests of a dual-system model of speech category learning. *Bilingualism: Language and Cognition*, **17**, 709–728.

- McDonald, S. and Zucchini, W. (1997). *Hidden Markov and other models for discrete-valued time series*. Chapman & Hall, London.
- Milosavljevic, M., Malmaud, J., Huth, A., Koch, C., and Rangel, A. (2010). The drift diffusion model can account for the accuracy and reaction time of value-based choices under high and low time pressure. *Judgment and Decision Making*, **5**, 437–449.
- Morris, J. S. (2015). Functional regression. *Annual Review of Statistics and Its Application*, **2**, 321–359.
- Müller, P., Quintana, F. A., Rosner, G. L., and Maitland, M. L. (2013). Bayesian inference for longitudinal data with non-parametric treatment effects. *Biostatistics*, **15**, 341–352.
- Navarro, D. J. and Fuss, I. G. (2009). Fast and accurate calculations for first-passage times in Wiener diffusion models. *Journal of Mathematical Psychology*, **53**, 222–230.
- Neal, R. M. (2003). Slice sampling. *The Annals of Statistics*, **31**, 705–767.
- Nguyen, X. and Gelfand, A. E. (2011). The Dirichlet labeling process for clustering functional data. *Statistica Sinica*, **21**, 1249–1289.
- Nguyen, X. and Gelfand, A. E. (2014). Bayesian nonparametric modeling for functional analysis of variance. *Annals of the Institute of Statistical Mathematics*, **66**, 495–526.
- Paulon, G. and Sarkar, A. (2020+). Bayesian longitudinal functional mixed models with time-varying predictor influences. *In preparation*.
- Paulon, G., Reetzke, R., Chandrasekaran, B., and Sarkar, A. (2019). Functional logistic mixed-effects models for learning curves from longitudinal binary data. *Journal of Speech, Language, and Hearing Research*, **62**, 543–553.
- Petrone, S., Guindani, M., and Gelfand, A. E. (2009). Hybrid Dirichlet mixture models for functional data. *Journal of the Royal Statistical Society: Series B (Statistical Methodology)*, **71**, 755–782.
- Polson, N. G. and Scott, J. G. (2012). On the half-Cauchy prior for a global scale parameter. *Bayesian Analysis*, **7**, 887–902.
- Purcell, B. A. (2013). *Neural mechanisms of perceptual decision making*. Vanderbilt University.
- Quintana, F. A., Johnson, W. O., Waetjen, L. E., and B. Gold, E. (2016). Bayesian nonparametric longitudinal data analysis. *Journal of the American Statistical Association*, **111**, 1168–1181.
- Rabiner, L. (1989). A tutorial on hidden Markov models and selected applications in speech recognition. *IEEE*, **77**, 257–286.

- Ramsay, J. O. and Silverman, B. W. (2007). *Applied functional data analysis: methods and case studies*. Springer.
- Ratcliff, R. (1978). A theory of memory retrieval. *Psychological review*, **85**, 59.
- Ratcliff, R. and McKoon, G. (2008). The diffusion decision model: Theory and data for two-choice decision tasks. *Neural Computation*, **20**, 873–922.
- Ratcliff, R. and Rouder, J. N. (1998). Modeling response times for two-choice decisions. *Psychological Science*, **9**, 347–356.
- Ratcliff, R., Smith, P. L., Brown, S. D., and McKoon, G. (2016). Diffusion decision model: Current issues and history. *Trends in Cognitive Sciences*, **20**, 260–281.
- Reetzke, R., Xie, Z., Llanos, F., and Chandrasekaran, B. (2018). Tracing the trajectory of sensory plasticity across different stages of speech learning in adulthood. *Current Biology*, **28**, 1419–1427.
- Ross, S. M., Kelly, J. J., Sullivan, R. J., Perry, W. J., Mercer, D., Davis, R. M., Washburn, T. D., Sager, E. V., Boyce, J. B., and Bristow, V. L. (1996). *Stochastic processes*. Wiley New York.
- Schall, J. D. (2001). Neural basis of deciding, choosing and acting. *Nature Reviews Neuroscience*, **2**, 33.
- Scott, S. L. (2002). Bayesian methods for hidden Markov models recursive computing in the 21st century. *Journal of the American Statistical Association*, **97**, 337–351.
- Singer, J. D., Willett, J. B., Willett, J. B., *et al.* (2003). *Applied longitudinal data analysis: Modeling change and event occurrence*. Oxford university press.
- Smith, P. L. and Ratcliff, R. (2004). Psychology and neurobiology of simple decisions. *Trends in Neurosciences*, **27**, 161–168.
- Smith, P. L. and Vickers, D. (1988). The accumulator model of two-choice discrimination. *Journal of Mathematical Psychology*, **32**, 135–168.
- Song, J. H., Skoe, E., Wong, P. C., and Kraus, N. (2008). Plasticity in the adult human auditory brainstem following short-term linguistic training. *Journal of Cognitive Neuroscience*, **20**, 1892–1902.
- Titsias, M. K. and Yau, C. (2014). Hamming ball auxiliary sampling for factorial hidden markov models. In *Advances in Neural Information Processing Systems*, pages 2960–2968.
- Tuerlinckx, F. (2004). The efficient computation of the cumulative distribution and probability density functions in the diffusion model. *Behavior Research Methods, Instruments, & Computers*, **36**, 702–716.
- Tuerlinckx, F., Maris, E., Ratcliff, R., and De Boeck, P. (2001). A comparison of four methods for simulating the diffusion process. *Behavior Research Methods, Instruments, & Computers*, **33**, 443–456.

- Usher, M. and McClelland, J. L. (2001). The time course of perceptual choice: The leaky, competing accumulator model. *Psychological Review*, **108**, 550.
- Van Gael, J., Saatci, Y., Teh, Y. W., and Ghahramani, Z. (2008). Beam sampling for the infinite hidden Markov model. In *Proceedings of the 25th International Conference on Machine Learning*, pages 1088–1095. ACM.
- Vandekerckhove, J. and Tuerlinckx, F. (2007). Fitting the Ratcliff diffusion model to experimental data. *Psychonomic Bulletin & Review*, **14**, 1011–1026.
- Vandekerckhove, J., Tuerlinckx, F., and Lee, M. D. (2008). A Bayesian approach to diffusion process models of decision-making. In *Proceedings of the 30th Annual Conference of the Cognitive Science Society*, pages 1429–1434. Washington, DC.
- Wang, J.-L., Chiou, J.-M., and Müller, H.-G. (2016). Functional data analysis. *Annual Review of Statistics and Its Application*, **3**, 257–295.
- Wang, Y., Spence, M. M., Jongman, A., and Sereno, J. A. (1999). Training american listeners to perceive mandarin tones. *The Journal of the Acoustical Society of America*, **106**, 3649–3658.
- Whitmore, G. and Seshadri, V. (1987). A heuristic derivation of the inverse gaussian distribution. *The American Statistician*, **41**, 280–281.
- Xie, Z., Reetzke, R., and Chandrasekaran, B. (2017). Stability and plasticity in neural encoding of linguistically relevant pitch patterns. *Journal of Neurophysiology*, **117**, 1409–1424.
- Zanella, G. (2019). Informed proposals for local MCMC in discrete spaces. *Journal of the American Statistical Association*, pages 1–14.

Supplementary Materials for

# Bayesian Semiparametric Longitudinal Drift-Diffusion Mixed Models for Tone Learning in Adults

Giorgio Paulon<sup>1</sup> (giorgio.paulon@utexas.edu)

Fernando Llanos<sup>2</sup> (f.llanos@pitt.edu)

Bharath Chandrasekaran<sup>2</sup> (b.chandra@pitt.edu)

Abhra Sarkar<sup>1</sup> (abhra.sarkar@utexas.edu)

<sup>1</sup>Department of Statistics and Data Sciences,  
University of Texas at Austin,  
2317 Speedway (D9800), Austin, TX 78712-1823, USA

<sup>2</sup>Department of Communication Sciences and Disorders,  
University of Pittsburgh,  
4028 Forbes Tower, Pittsburgh, PA 15260, USA

Supplementary materials present a review of current neurobiological models of speech processing, brief reviews of B-splines and fHMMs, details of the MCMC algorithm we designed to sample from the posterior, a review of linear ballistic accumulator models, and some additional figures.

## S.1 Neurobiology of Speech Learning

The acquisition of novel speech categories is a difficult task that engages multiple brain networks (Guediche *et al.*, 2014; Lim *et al.*, 2014; Feng *et al.*, 2018). In a typical laboratory-based speech training task, learners are guided with feedback to map non-native speech sounds onto linguistically relevant categories by pressing a button on the keyboard (Wang *et al.*, 1999; Maddox and Chandrasekaran, 2014; Reetzke *et al.*, 2018).

According to current models of speech processing, sound waves are transduced into fast subcortical oscillations and are then delivered to the primary auditory cortex for further processing (Chandrasekaran *et al.*, 2011; Giraud and Poeppel, 2012). Engaging a fronto-tempo-parietal network, the superior temporal gyrus (STG) then encodes the spectral and temporal features, and the superior temporal sulcus (STS) encodes the phonological-level information (sound properties that are meaningful in a particular language context) (Hickok and Poeppel, 2007; Rauschecker and Scott, 2009). STG and STS are connected to frontal and parietal areas, specifically, the dorsolateral prefrontal cortex (DLPC), the left inferior parietal (LIP), and the inferior frontal gyrus (IFG), that select, maintain, and refresh the sensory evidence collected over time (Salvata *et al.*, 2012; Xie and Myers, 2018). After a decision is made, feedback is used to guide stimulus-response associations by rewarding or penalizing specific decision activities, e.g. pressing the right button. The processing of this information is linked to a network mediated by the basal ganglia (BG) (Lim *et al.*, 2014), the orbitofrontal cortex (OFC) (O'Doherty *et al.*, 2001), and the anterior cingulate cortex (ACC) (Kennerley *et al.*, 2006). Neurons in the OFC respond selectively to rewards or aversive stimuli and process the relative preference for rewards. In the BG, correct decision actions are rewarded with discharges of dopamine that reinforce correct sound-to-category associations and contribute to the preparation and initiation of decision actions. The ACC contrasts information provided by feedback with previous history of actions to update and sustain the value of decision actions.

Studies have established links between the brain networks discussed above and different parameters in existing drift-diffusion models. Differences in drift rates have been related to activity in fronto-tempo-parietal areas supporting the collection, maintenance, and categorization of sensory input (e.g., DLPC, IFG, and LIP) (Serenio *et al.*, 2001; Rolls *et al.*, 2010; White *et al.*, 2014). Differences in decision thresholds have been associated with activity in a cortical-striatal network involved in the selection and preparation of decision actions (e.g., the striatum and SNT of the BG, and the premotor cortex) (Bogacz *et al.*, 2010; Cavanagh *et al.*, 2011; van Maanen *et al.*, 2011). Differences in non-decision times have been linked to activity in areas that process and update the expected value of decision actions (e.g., OFC and the ACC) (Forstmann *et al.*, 2010; Domenech and Dreher, 2010) and areas involved in perceptual encoding (e.g. auditory cortex and STG) and response execution (motor cortex) (Mulder *et al.*, 2014).

The drift-diffusion mixed model for accuracies and response times developed in this article, combined with simultaneously recorded imaging data, presents exciting new opportunities for validating the putative correspondence between model parameters and brain networks in speech category learning tasks, forming a major component of our planned future research.

## S.2 B-splines

In the main article, we employed quadratic B-spline bases in the construction of functional factorial HMMs. The construction of quadratic B-spline bases is detailed below (de Boor, 1978). Consider knot-points  $t_1 = t_2 = t_3 = A < t_4 < \dots < B = t_{K+3} = t_{K+4} = t_{K+5}$ , where  $t_{3:(K+3)}$  are equidistant with  $\delta = (t_4 - t_3)$ . For  $j = 3, 4, \dots, (K+2)$ , quadratic B-splines  $b_{2,j}$  are then defined as

$$b_{2,j}(X) = \begin{cases} \{(X - t_{j-1})/\delta\}^2/2 & \text{if } t_{j-1} \leq X < t_j, \\ -\{(X - t_j)/\delta\}^2 + (X - t_j)/\delta + 1/2 & \text{if } t_j \leq X < t_{j+2}, \\ \{1 - (X - t_{j+2})/\delta\}^2 & \text{if } t_{j+2} \leq X < t_{j+3}, \\ 0 & \text{otherwise.} \end{cases}$$

The components at the ends are likewise defined as

$$\begin{aligned} b_{2,1}(X) &= \begin{cases} \{1 - (X - t_1)/\delta\}^2/2 & \text{if } t_3 \leq X < t_4, \\ 0 & \text{otherwise.} \end{cases} \\ b_{2,2}(X) &= \begin{cases} -\{(X - t_3)/\delta\}^2 + (X - t_4)/\delta + 1/2 & \text{if } t_3 \leq X < t_4, \\ \{1 - (X - t_4)/\delta\}^2/2 & \text{if } t_4 \leq X < t_5, \\ 0 & \text{otherwise.} \end{cases} \\ b_{2,K+1}(X) &= \begin{cases} \{(X - t_{K+1})/\delta\}^2/2 & \text{if } t_{K+1} \leq X < t_{K+2}, \\ -\{(X - t_{K+2})/\delta\}^2 + (X - t_{K+2})/\delta + 1/2 & \text{if } t_{K+2} \leq X < t_{K+3}, \\ 0 & \text{otherwise.} \end{cases} \\ b_{2,K+2}(X) &= \begin{cases} \{(X - t_{K+2})/\delta\}^2/2 & \text{if } t_{K+2} \leq X < t_{K+3}, \\ 0 & \text{otherwise.} \end{cases} \end{aligned}$$



### S.3 Factorial HMM (fHMM)

The basic HMM (Frühwirth-Schnatter, 2006; McDonald and Zucchini, 1997, etc.) consists of two processes: an *observed* process  $\{\mathbf{y}_t\}$  recorded sequentially over a set of discrete time points  $t = 1, 2, \dots, T$  and an associated *hidden* process  $\{z_t\}$  which evolves according to a first order Markov chain with discrete state space. Specifically, an HMM makes the following set of conditional independence assumptions to model the hidden and the observed processes

$$\begin{aligned} p(z_t \mid \mathbf{z}_{1:(t-1)}) &= p(z_t \mid z_{t-1}), \\ p(\mathbf{y}_t \mid \mathbf{y}_{1:(t-1)}, \mathbf{z}_{1:t}) &= p(y_t \mid z_t). \end{aligned}$$

The distributions  $p(z_t \mid z_{t-1})$  and  $p(y_t \mid z_t)$  are often referred to as the *transition distribution* and the *emission distribution*, respectively.

In factorial HMMs (Ghahramani and Jordan, 1997), the latent states are represented by a collection of variables  $\{\mathbf{z}_t\} = \{(z_t^{(1)}, \dots, z_t^{(L)})\}$  where each component  $\{z_t^{(\ell)}\}$  now evolves according to a first order Markov chain with discrete state spaces, and the *observed* process  $\{y_t\}$  is observed sequentially as before over a set of discrete time points  $t = 1, 2, \dots, T$ . An fHMM thus makes the following set of conditional independence assumptions to model the hidden and the observed processes

$$\begin{aligned} p(\mathbf{z}_t \mid \mathbf{z}_{1:(t-1)}) &= \prod_{\ell=1}^L p(z_t^{(\ell)} \mid z_{t-1}^{(\ell)}), \\ p(y_t \mid \mathbf{y}_{1:(t-1)}, \mathbf{z}_{1:t}) &= p(\mathbf{y}_t \mid \mathbf{z}_t) = p(y_t \mid z_t^{(1)}, \dots, z_t^{(L)}). \end{aligned}$$

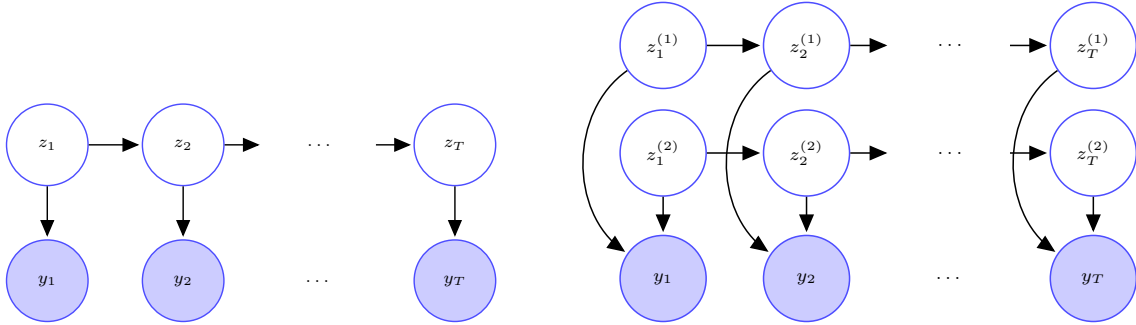


Figure S.1: Left panel: graph of an HMM. Right panel: graph of an fHMM with two layers.

In our work, we adapted the basic fHMM to characterize local influences of the categorical predictor in longitudinal functional models. In the drift-diffusion model of Section 4, for each input tone  $s \in \{1, \dots, d_1\}$ , we introduced an fHMM  $\{\mathbf{z}_k^{(s)} = (z_k^{(1,s)}, \dots, z_k^{(d_0,s)})\}$  with  $d_0$  layers, one for each level of the response  $d$ . Conditional on  $z_k^{(d,s)} = z_k$ , we then associated the coefficients  $\beta_{k,d,s}$  of a predictor dependent B-spline mixture model with atoms  $\beta_{k,z_k}^*$ . Specifically, we let

$$\begin{aligned} p(\mathbf{z}_k^{(s)} \mid \mathbf{z}_{1:(k-1)}^{(s)}) &= \prod_{d=1}^{d_0} p(z_k^{(d,s)} \mid z_{k-1}^{(d,s)}), \\ \{\beta_{k,d,s} \mid z_k^{(d,s)} = z_k\} &= \beta_{k,z_k}^*. \end{aligned}$$

## S.4 Locally Informed Hamming Ball Sampler

Forward-backward (or backward-forward) algorithms for HMMs rely on passing messages forward (or backward) and then sampling backward (or forward) (Rabiner, 1989; Scott, 2002). While adapting such algorithms to fHMMs, the requirement to sum over all possible configurations in computing the messages becomes a challenge. Hamming ball samplers for fHMMs (Titsias and Yau, 2014) avoid this computationally expensive step by introducing and conditioning on an auxiliary variable that restricts the sampling to only a slice (Neal, 2003) of the entire high-dimensional space. In doing so, the sampler also allows localized joint updating of all constituent chains, making it less prone to get trapped in local modes.

Let  $h(\mathbf{z}_t, \mathbf{v}_t) = \sum_{\ell=1}^L 1\{z_t^\ell \neq v_t^\ell\}$  denote the Hamming distance between the vectors  $\mathbf{z}_t = (z_t^{(1)}, \dots, z_t^{(L)})^T$  and  $\mathbf{v}_t = (v_t^{(1)}, \dots, v_t^{(L)})^T$  and  $\mathcal{H}_m(\mathbf{z}_t) = \{\mathbf{v}_t : h(\mathbf{z}_t, \mathbf{v}_t) \leq m\}$  denote a Hamming ball of radius  $m$  around  $\mathbf{z}_t$ .

Consider an fHMM, as shown in Figure S.1 but with  $L$  component chains each with state space  $\{1, \dots, d\}$ . Introducing an auxiliary variable  $\mathbf{v}$  following a conditional probability distribution  $p(\mathbf{v} | \mathbf{z}) = \prod_{t=1}^T p(\mathbf{v}_t | \mathbf{z}_t)$ , the augmented joint model becomes  $p(\mathbf{y}, \mathbf{z}, \mathbf{v}) = p(\mathbf{v} | \mathbf{z})p(\mathbf{y} | \mathbf{z})p(\mathbf{z}) = \{\prod_{t=1}^T p(\mathbf{v}_t | \mathbf{z}_t)p(\mathbf{y}_t | \mathbf{z}_t)\}p(\mathbf{z}_1)\prod_{t=2}^T p(\mathbf{z}_t | \mathbf{z}_{t-1})$ . Sampling  $\mathbf{v}$  from the posterior can then be done by sampling independently from the full conditionals  $p(\mathbf{v}_t | \mathbf{z}_t)$ . Sampling  $\mathbf{z}$  from the posterior can still be carried out using forward-backward (or backward-forward) message passing algorithms but with the augmented full conditional  $p(\mathbf{z} | \mathbf{y}, \mathbf{v}) \propto \{\prod_{t=1}^T p(\mathbf{v}_t | \mathbf{z}_t)p(\mathbf{y}_t | \mathbf{z}_t)\}\{\prod_{t=2}^T p(\mathbf{z}_t | \mathbf{z}_{t-1})\}p(\mathbf{z}_1)$ . The set of possible configurations needed to compute the messages at time  $t$  is now restricted to the support of  $p(\mathbf{v}_t | \mathbf{z}_t)$ . If this can be made much smaller compared to the original size of the state space, computational burden can be greatly reduced.

The Hamming ball algorithm does this by setting  $p(\mathbf{v}_t | \mathbf{z}_t) \propto 1\{\mathbf{v}_t \in \mathcal{H}_m(\mathbf{z}_t)\}$ , that is, by sampling the  $\mathbf{v}_t$ 's uniformly from  $\mathcal{H}_m(\mathbf{z}_t)$ . By symmetry, since  $\mathbf{v}_t \in \mathcal{H}_m(\mathbf{z}_t)$  if and only if  $\mathbf{z}_t \in \mathcal{H}_m(\mathbf{v}_t)$ , the support of each  $\mathbf{z}_t$  in the full conditional  $p(\mathbf{z} | \mathbf{y}, \mathbf{v})$  is then restricted only to  $\mathcal{H}_m(\mathbf{v}_t)$ .

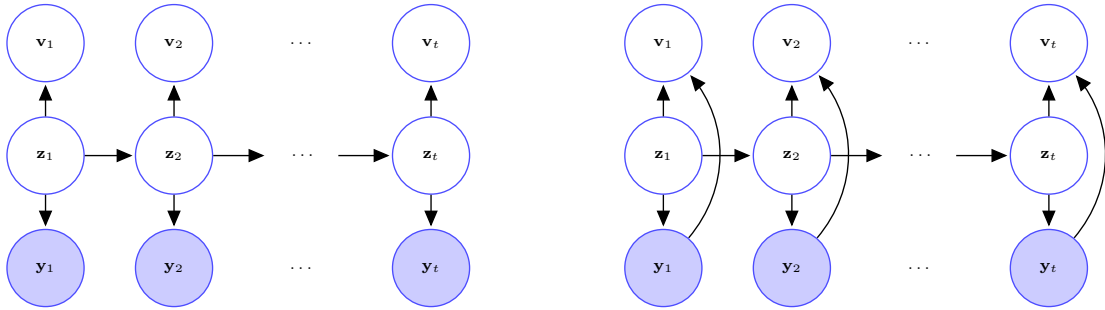


Figure S.2: Graph of a Hamming ball sampler (left panel) and a locally informed Hamming ball sampler (right panel) for fHMM.

The Hamming ball sampler is still limited in its ability to efficiently explore the neighborhood of  $\mathbf{z}_t$  as it blindly proposes new values along arbitrarily chosen directions within the ball. More informed moves can be proposed utilizing the information contained in the like-

likelihood function (Zanella, 2019). For instance,  $p(\mathbf{v}_t | \mathbf{z}_t, \mathbf{y}_t) \propto g\{p(\mathbf{y}_t | \mathbf{v}_t)\}1\{\mathbf{v}_t \in \mathcal{H}_m(\mathbf{z}_t)\}$ , for proper choices of  $g(\cdot)$ , favors moves along directions that increase the conditional likelihood  $p(\mathbf{y}_t | \mathbf{v}_t)$  (Figure S.2 and Figure S.3). The augmented joint model now becomes  $p(\mathbf{y}, \mathbf{z}, \mathbf{v}) = p(\mathbf{v} | \mathbf{y}, \mathbf{z})p(\mathbf{y} | \mathbf{z})p(\mathbf{z}) = \{\prod_{t=1}^T p(\mathbf{v}_t | \mathbf{y}_t, \mathbf{z}_t)p(\mathbf{y}_t | \mathbf{z}_t)\}\{\prod_{t=2}^T p(\mathbf{z}_t | \mathbf{z}_{t-1})\}p(\mathbf{z}_1)$ . Sampling  $\mathbf{z}$  from the posterior can be carried out using message passing algorithms as before with each  $\mathbf{z}_t$  restricted to  $\mathcal{H}_m(\mathbf{v}_t)$  but with the updated full conditionals  $p(\mathbf{z} | \mathbf{y}, \mathbf{v}) \propto \{\prod_{t=1}^T p(\mathbf{v}_t | \mathbf{z}_t, \mathbf{y}_t)p(\mathbf{y}_t | \mathbf{z}_t)\}\{\prod_{t=2}^T p(\mathbf{z}_t | \mathbf{z}_{t-1})\}p(\mathbf{z}_1)$ .

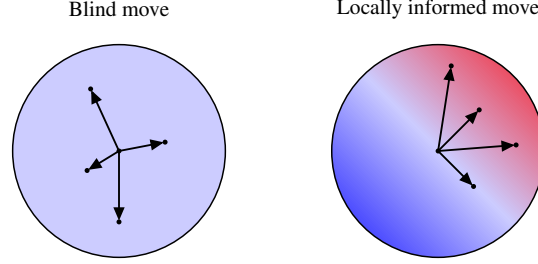


Figure S.3: The basic Hamming ball sampler (left) and the locally informed Hamming ball sampler (right). The circles represent the Hamming balls, its center being the current state  $\mathbf{z}_t$ . The points inside the Hamming balls are colored according to value of the likelihood at that point. Larger values of the likelihood are represented here in warmer hues. The basic sampler proposes moves along arbitrarily chosen directions. The locally informed sampler proposes moves along directions of increasing likelihood with higher probability.

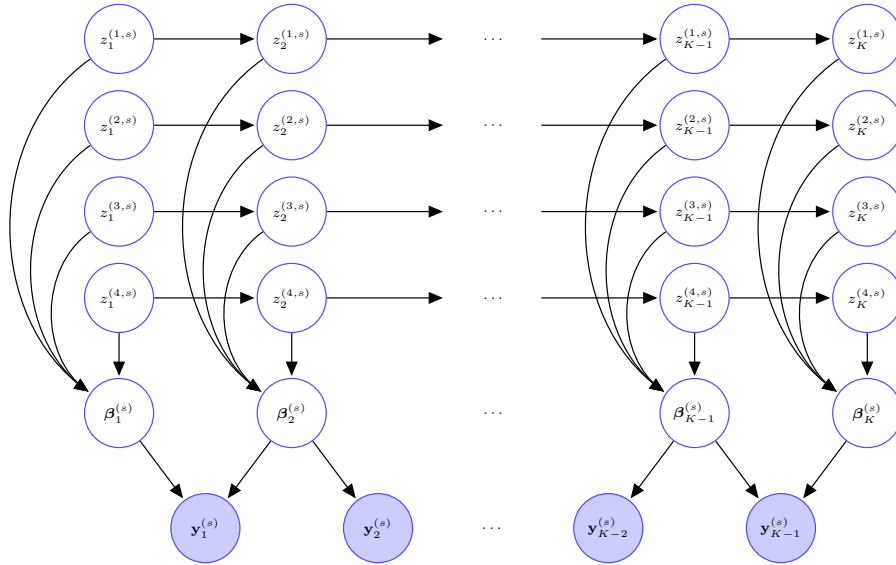


Figure S.4: Graph of the proposed longitudinal drift-diffusion mixed model for tone learning with  $\beta_k^{(1,s)}, \dots, \beta_k^{(4,s)}$  collected in single nodes  $\beta_k^{(s)}$  for each  $k$ .

## S.5 Posterior Inference

### S.5.1 Prior Hyper-parameters and MCMC Initializations

The fixed effects parameters of the mixed effects model (1) are initialized at the estimates obtained by fitting the fixed effects model  $\{\theta_x^{(i)}(t) \mid x_{i,\ell,t} = x\} = f_x(t)$ . The random effects are instead initialized to zero. The initialization of the MCMC chain for the drift-diffusion mixed model also mimics this strategy. The clustering configuration is initialized with all the success curves in different clusters, and all the failure curves in the same cluster.

Crucial hyper-parameters are the mean and the standard deviation for the prior term of the unassigned components of  $\beta_x$ , that is, the second term in the prior (4) in the main paper. In the mixed effects model (1), we can use an empirical Bayes type approach to choose  $\mu_{\beta,0}, \sigma_{\beta,0}^2$ . Since  $\beta_x$  are the spline coefficients for the mean function of the observations with covariate  $x$ , we can simply initialize them to the empirical mean and empirical variance of the observations at every time point. In the drift-diffusion mixed model, the same strategy is not available because  $\beta_{\mu,x}$  and  $\beta_{b,x}$  are the spline coefficients associated to latent functions. However, we can still try to use the data to find a range of plausible values for these parameters. In fact, as discussed in Section 4, boundary and drift parameters are related to the first two moments of the response times. Thus, we use the empirical distributions of response times at every time point to define plausible moments for the normal distribution in (4). The concentration parameters  $\alpha^{(C)}$  and  $\alpha^{(I)}$  were assigned a Gamma(1, 1) prior as recommended in Escobar and West (1995).

### S.5.2 Posterior Computation

Posterior inference for the longitudinal mixed model framework developed in Section 3 in the main paper, as well as its drift-diffusion model adaptation described in Section 4, is based on samples drawn from the posterior using a message passing MCMC algorithm.

In what follows,  $\zeta$  denotes a generic variable that collects all other variables not explicitly mentioned, including the data points. Also,  $p_0$  will sometimes be used as a generic for a prior distribution without explicitly mentioning its hyper-parameters. The sampler for the drift diffusion model of Section 4 comprises the following steps.

1. Update the offset parameters  $\delta_s, s = 1, \dots, d_0$ . The full conditionals  $p(\delta_s \mid \zeta) \propto p_0(\delta_s)L(\mathbf{y} \mid \mathbf{s}, \boldsymbol{\theta})$  do not have closed forms. Metropolis-Hastings (MH) steps with log-normal proposals centered on the previous sampled values are used to update these parameters.
2. Jointly update the drift and boundary spline coefficients  $(\beta_{\mu,k,z_k}^*, \beta_{b,k,z_k}^*), k = 1, \dots, K$ .
  - (a) If the parameters are assigned to one of the clusters, the full conditionals do not have closed forms. MH steps are therefore used with the smoothness inducing priors (4) on  $(\beta_{\mu,k,z_k}^*, \beta_{b,k,z_k}^*)$  as the proposal distributions.

- (b) If the parameters are not assigned to any of the clusters, the full conditional distribution is the second term of the prior in (4).

3. Update the latent cluster assignments  $\mathbf{z}_k^{(s)} = (z_k^{(1,s)}, \dots, z_k^{(4,s)})^T$ :

- (a) Sample the auxiliary variables  $\mathbf{v}_k^{(s)} = (v_k^{(1,s)}, \dots, v_k^{(4,s)})^T$  as

$$p(\mathbf{v}_k^{(s)} \mid \mathbf{z}_k^{(s)}, \mathbf{z}_{k+1}^{(s)}, \mathbf{y}_k^{(s)}, \boldsymbol{\zeta}) \propto g\{p(\mathbf{y}_k^{(s)} \mid \mathbf{v}_k^{(s)}, \mathbf{z}_{k+1}^{(s)}, \boldsymbol{\zeta})\} 1\{\mathbf{v}_k^{(s)} \in \mathcal{H}_m(\mathbf{z}_k^{(s)})\}, \quad k = 1, \dots, K-1,$$

$$p(\mathbf{v}_K^{(s)} \mid \mathbf{z}_K^{(s)}, \boldsymbol{\zeta}) \propto 1\{\mathbf{v}_K^{(s)} \in \mathcal{H}_m(\mathbf{z}_K^{(s)})\}.$$

- (b) Back-propagate the messages  $m_k(\mathbf{z}_k^{(s)}) = p(\mathbf{y}_{k:(K-1)}^{(s)}, \mathbf{v}_{k:K}^{(s)} \mid \mathbf{z}_k^{(s)}, \boldsymbol{\zeta})$  using the recursion

$$\begin{aligned} m_k(\mathbf{z}_k^{(s)}) &= p(\mathbf{y}_{k:(K-1)}^{(s)}, \mathbf{v}_{k:K}^{(s)} \mid \mathbf{z}_k^{(s)}, \boldsymbol{\zeta}) \\ &= \sum_{\mathbf{z}_{k+1}^{(s)}} p(\mathbf{y}_{k:(K-1)}^{(s)}, \mathbf{v}_{k:K}^{(s)} \mid \mathbf{z}_k^{(s)}, \mathbf{z}_{k+1}^{(s)}, \boldsymbol{\zeta}) p(\mathbf{z}_{k+1}^{(s)} \mid \mathbf{z}_k^{(s)}, \boldsymbol{\zeta}) \\ &= \sum_{\mathbf{z}_{k+1}^{(s)}} p(\mathbf{y}_k^{(s)}, \mathbf{v}_k^{(s)} \mid \mathbf{z}_k^{(s)}, \mathbf{z}_{k+1}^{(s)}, \boldsymbol{\zeta}) p(\mathbf{y}_{(k+1):(K-1)}^{(s)}, \mathbf{v}_{(k+1):K}^{(s)} \mid \mathbf{z}_k^{(s)}, \mathbf{z}_{k+1}^{(s)}, \boldsymbol{\zeta}) p(\mathbf{z}_{k+1}^{(s)} \mid \mathbf{z}_k^{(s)}, \boldsymbol{\zeta}) \\ &= \sum_{\mathbf{z}_{k+1}^{(s)}} p(\mathbf{y}_k^{(s)}, \mathbf{v}_k^{(s)} \mid \mathbf{z}_k^{(s)}, \mathbf{z}_{k+1}^{(s)}, \boldsymbol{\zeta}) p(\mathbf{y}_{(k+1):(K-1)}^{(s)}, \mathbf{v}_{(k+1):K}^{(s)} \mid \mathbf{z}_{k+1}^{(s)}, \boldsymbol{\zeta}) p(\mathbf{z}_{k+1}^{(s)} \mid \mathbf{z}_k^{(s)}, \boldsymbol{\zeta}) \\ &= \sum_{\mathbf{z}_{k+1}^{(s)}} p(\mathbf{v}_k^{(s)} \mid \mathbf{z}_k^{(s)}, \mathbf{z}_{k+1}^{(s)}, \mathbf{y}_k^{(s)}, \boldsymbol{\zeta}) p(\mathbf{y}_k^{(s)} \mid \mathbf{z}_k^{(s)}, \mathbf{z}_{k+1}^{(s)}, \boldsymbol{\zeta}) p(\mathbf{z}_{k+1}^{(s)} \mid \mathbf{z}_k^{(s)}, \boldsymbol{\zeta}) m_{k+1}(\mathbf{z}_{k+1}^{(s)}), \\ &\propto \sum_{\mathbf{z}_{k+1}^{(s)} \in \mathcal{H}_m(\mathbf{v}_{k+1}^{(s)})} g\{p(\mathbf{y}_k^{(s)} \mid \mathbf{v}_k^{(s)}, \mathbf{z}_{k+1}^{(s)}, \boldsymbol{\zeta})\} 1\{\mathbf{v}_k^{(s)} \in \mathcal{H}_m(\mathbf{z}_k^{(s)})\} p(\mathbf{y}_k^{(s)} \mid \mathbf{z}_k^{(s)}, \mathbf{z}_{k+1}^{(s)}, \boldsymbol{\zeta}) p(\mathbf{z}_{k+1}^{(s)} \mid \mathbf{z}_k^{(s)}, \boldsymbol{\zeta}) m_{k+1}(\mathbf{z}_{k+1}^{(s)}), \end{aligned}$$

starting with the final condition  $m_K(\mathbf{z}_K^{(s)}) = 1\{\mathbf{z}_K^{(s)} \in \mathcal{H}_m(\mathbf{v}_K^{(s)})\}$ .

- (c) Sample the latent cluster assignments forward one step at a time from

$$p(\mathbf{z}_{1:K}^{(s)} \mid \mathbf{y}_{1:(K-1)}^{(s)}, \mathbf{v}_{1:K}^{(s)}, \boldsymbol{\zeta}) = p(\mathbf{z}_K^{(s)} \mid \mathbf{z}_{1:(K-1)}^{(s)}, \mathbf{y}_{1:(K-1)}^{(s)}, \mathbf{v}_{1:K}^{(s)}, \boldsymbol{\zeta}) \cdots p(\mathbf{z}_1^{(s)} \mid \mathbf{y}_{1:(K-1)}^{(s)}, \mathbf{v}_{1:K}^{(s)}, \boldsymbol{\zeta}),$$

where

$$\begin{aligned} p(\mathbf{z}_k^{(s)} \mid \mathbf{z}_{1:(k-1)}^{(s)}, \mathbf{y}_{1:(K-1)}^{(s)}, \mathbf{v}_{1:K}^{(s)}, \boldsymbol{\zeta}) &\propto p(\mathbf{y}_{k:(K-1)}^{(s)}, \mathbf{v}_{k:K}^{(s)} \mid \mathbf{z}_{1:k}^{(s)}, \boldsymbol{\zeta}) p(\mathbf{z}_k^{(s)} \mid \mathbf{z}_{1:(k-1)}^{(s)}, \boldsymbol{\zeta}) \\ &= p(\mathbf{y}_{1:(k-2)}^{(s)}, \mathbf{v}_{1:(k-2)}^{(s)} \mid \mathbf{z}_{1:k}^{(s)}, \boldsymbol{\zeta}) p(\mathbf{y}_{k-1}^{(s)}, \mathbf{v}_{k-1}^{(s)} \mid \mathbf{z}_{k-1}^{(s)}, \mathbf{z}_k^{(s)}, \boldsymbol{\zeta}) p(\mathbf{y}_{k:(K-1)}^{(s)}, \mathbf{v}_{k:K}^{(s)} \mid \mathbf{z}_k^{(s)}, \boldsymbol{\zeta}) p(\mathbf{z}_k^{(s)} \mid \mathbf{z}_{1:(k-1)}^{(s)}, \boldsymbol{\zeta}) \\ &\propto p(\mathbf{y}_{k-1}^{(s)}, \mathbf{v}_{k-1}^{(s)} \mid \mathbf{z}_{k-1}^{(s)}, \mathbf{z}_k^{(s)}, \boldsymbol{\zeta}) p(\mathbf{z}_k^{(s)} \mid \mathbf{z}_{1:(k-1)}^{(s)}, \boldsymbol{\zeta}) m_k(\mathbf{z}_k^{(s)}) \\ &= p(\mathbf{v}_{k-1}^{(s)} \mid \mathbf{z}_{k-1}^{(s)}, \mathbf{z}_k^{(s)}, \mathbf{y}_{k-1}^{(s)}, \boldsymbol{\zeta}) p(\mathbf{y}_{k-1}^{(s)} \mid \mathbf{z}_{k-1}^{(s)}, \mathbf{z}_k^{(s)}, \boldsymbol{\zeta}) p(\mathbf{z}_k^{(s)} \mid \mathbf{z}_{k-1}^{(s)}, \boldsymbol{\zeta}) m_k(\mathbf{z}_k^{(s)}) \\ &\propto g\{p(\mathbf{y}_{k-1}^{(s)} \mid \mathbf{v}_{k-1}^{(s)}, \mathbf{z}_k^{(s)}, \boldsymbol{\zeta})\} p(\mathbf{y}_{k-1}^{(s)} \mid \mathbf{z}_{k-1}^{(s)}, \mathbf{z}_k^{(s)}, \boldsymbol{\zeta}) p(\mathbf{z}_k^{(s)} \mid \mathbf{z}_{k-1}^{(s)}, \boldsymbol{\zeta}) m_k(\mathbf{z}_k^{(s)}). \end{aligned}$$

4. Update the cluster specific fixed effects spline coefficients:

$$\begin{aligned} (\beta_{\mu,k,x} \mid z_k^{(x)} = z_k, \zeta) &\sim 1\{\beta_{\mu,k,x} = \beta_{\mu,k,z_k}^*\}, \quad k = 1, \dots, K. \\ (\beta_{b,k,x} \mid z_k^{(x)} = z_k, \zeta) &\sim 1\{\beta_{b,k,x} = \beta_{b,k,z_k}^*\}, \quad k = 1, \dots, K. \end{aligned}$$

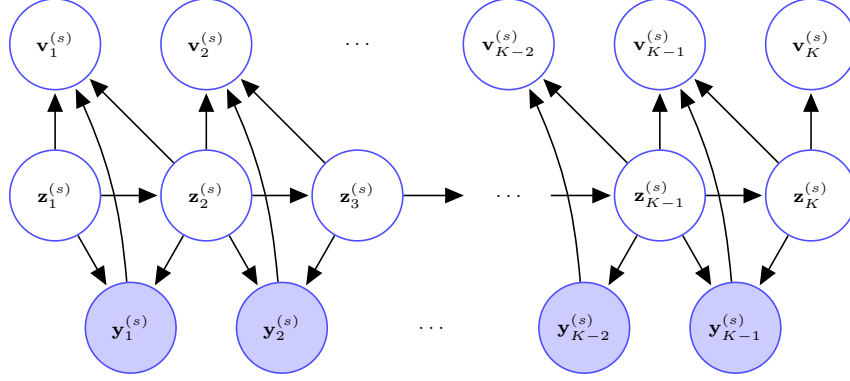


Figure S.5: Locally informed Hamming ball sampling of the latent states in our tone-learning longitudinal drift-diffusion mixed model. See also Figure 8 in the main paper.

5. Update the transition probability matrices:

$$\begin{aligned} (\pi_z^{(C)} \mid \zeta) &\sim \text{Dir}(\alpha^{(C)}/z_{\max} + n_{z,1}^{(C)}, \dots, \alpha^{(C)}/z_{\max} + n_{z,z_{\max}}^{(C)}) \\ (\pi_z^{(I)} \mid \zeta) &\sim \text{Dir}(\alpha^{(I)}/z_{\max} + n_{z,1}^{(I)}, \dots, \alpha^{(I)}/z_{\max} + n_{z,z_{\max}}^{(I)}), \end{aligned}$$

where  $n_{z,z'}^{(C)} = \sum_k 1\{z_k^{(x)} = z, z_{k+1}^{(x)} = z'\}$  is the number of transitions from  $z$  to  $z'$  for the HMMs associated with the correct identification of the tones, that is, with  $x$  s.t.  $d = s$ . A similar definition holds for  $n_{z,z'}^{(I)}$ .

6. Update the cluster specific smoothness parameter

$$p(\sigma_{\beta_{\mu,1}}^2 \mid \zeta) \propto (\sigma_{\beta_{\mu,1}})^{-Kc_x} \exp\left(-\frac{1}{2\sigma_{\beta_{\mu,1}}^2} \sum_x \beta_{\mu,x}^T \mathbf{P}_u \beta_{\mu,x}\right) p_0(\sigma_{\mu,u,a}^2).$$

MH steps with log-normal proposals centered on the previous sampled values are used to update these parameters.

7. Update the random effects spline coefficients  $\beta_{\mu,k,u}^{(i)}$  and  $\beta_{b,k,u}^{(i)}$ . The full conditional does not have a closed form, therefore a MH step with normal proposal centered on the previous value was used.

8. Update the random effects variance parameters  $\sigma_{\mu,u,a}^2$ ,  $\sigma_{\mu,u,s}^2$ ,  $\sigma_{b,u,a}^2$  and  $\sigma_{b,u,s}^2$ :  
The full conditional for  $\sigma_{\mu,u,a}^2$  is given by

$$p(\sigma_{\mu,u,a}^2 \mid \zeta) \propto \det(\sigma_{\mu,u,s}^{-2} \mathbf{P}_u + \sigma_{\mu,u,a}^{-2} \mathbf{I}_K)^{n/2} \exp\left(-\frac{1}{2\sigma_{\mu,u,a}^2} \sum_{i=1}^n \beta_{\mu,u}^{(i)T} \mathbf{P}_u \beta_{\mu,u}^{(i)}\right) p_0(\sigma_{\mu,u,a}^2).$$

Analogous expressions can be found for the full conditionals of  $\sigma_{\mu,u,s}^2$ ,  $\sigma_{b,u,a}^2$  and  $\sigma_{b,u,s}^2$ . MH steps with log-normal proposals centered on the previous sampled values are used to update these parameters.

The main challenge here arises from the nonconjugacy of the inverse Gaussian distribution based likelihood function, requiring MH steps for updating  $\delta_s$ ,  $\beta_{b,k,z_k}^*$ ,  $\beta_{\mu,k,z_k}^*$ . We employed the adaptive MH algorithm (Roberts and Rosenthal, 2009) for updating  $\delta_s$  and the variance parameters, avoiding the difficult task of choosing the parameters of their proposal distributions while also improving mixing. Specifically, for every batch of 50 iterations, we inflate or deflate the standard deviation of the proposal distribution in such a way to achieve an optimal acceptance rate of 44% (Roberts *et al.*, 2001). The adaptive MH could not be employed for the cluster specific parameters ( $\beta_{b,k,z_k}^*$ ,  $\beta_{\mu,k,z_k}^*$ ) due to label switching, so we used tempered MH. For the proposal distributions for ( $\beta_{b,k,z_k}^*$ ,  $\beta_{\mu,k,z_k}^*$ ), we used the smoothness inducing conditional prior distributions  $p_0(\beta_{\mu,k,z_k}^* | \beta_{\mu,k-1}^*) \times p_0(\beta_{b,k,z_k}^* | \beta_{b,k-1}^*)$ . Since the conditioning variables  $\beta_{\mu,k-1}^*$  and  $\beta_{b,k-1}^*$  are also updated at every iteration, the values sampled from the smoothness inducing priors are frequently accepted.

Based on  $M$  thinned samples  $\{\theta^{(m)}\}_{m=1}^M$  drawn from the posterior after the burn-in, the individual level drift parameters in the drift-diffusion mixed model are estimated as

$$\mu_x^{(i)}(t) = \exp\{f_{\mu,x}(t) + u_\mu^{(i)}(t)\} = \frac{1}{M} \sum_{m=1}^M \exp\{\hat{f}_{\mu,x}^{(m)}(t) + \hat{u}_\mu^{(i,m)}(t)\},$$

where  $\hat{f}_{\mu,x}^{(m)}(t) = \sum_{k=1}^K \beta_{\mu,k,z_k}^{*(m)} b_k(t)$ ,  $\hat{u}_\mu^{(i,m)}(t) = \sum_{k=1}^K \beta_{k,u,\mu}^{(i,m)} b_k(t)$  etc. The population level drift parameters are likewise estimated as

$$\begin{aligned} \mu_x(t) &= \int \exp\{f_{\mu,x}(t) + u_\mu^{(i)}(t)\} f\{u_\mu^{(i)}(t)\} du_\mu^{(i)}(t) = \exp\left[f_{\mu,x}(t) + \frac{\text{var}\{u_\mu^{(i)}(t)\}}{2}\right] \\ &= \frac{1}{M} \sum_{m=1}^M \exp\left\{\hat{f}_{\mu,x}^{(m)}(t) + \frac{\text{var}\{\hat{u}_\mu^{(i,m)}(t)\}}{2}\right\}, \end{aligned}$$

The results reported in this article are all based on 5,000 MCMC iterations with the initial 2,000 iterations discarded as burn-in. The remaining samples were further thinned by an interval of 5. We programmed in R. The codes are available as part of the supplementary materials. A ‘readme’ file, providing additional details for a practitioner, is also included in the supplementary materials. In all experiments, the posterior samples produced very stable estimates of the population and individual level parameters of interest. MCMC diagnostic checks were not indicative of any convergence or mixing issues.

## S.6 Linear Ballistic Accumulator Model

We present here a review of the LBA model (Brown and Heathcote, 2008) for easy reference with some repetition from the main paper to make this section relatively self-contained.

The LBA model is a popular framework for studying neural mechanisms underlying choice between multiple alternatives. Similar to our model, it uses independent evidence accumulators starting at  $\delta_s$  that continue until a response boundary  $b_s$  is reached. The accumulator that first reaches the boundary corresponds to the decision outcome, and the time at which the boundary is reached is the response time. The evidence, however, accumulates linearly at the rate  $\mu_{d,s}$ , reaching the boundary  $b_s$  precisely at time  $\tau_d = b_s/\mu_{d,s}$ . To explain trial-by-trial variability, the LBA model assumes that the slopes  $\mu$  for different trials are random draws from a Normal( $m_{d,s}, v_{d,s}$ ) distribution. The cumulative distribution function for the boundary crossing time  $\tau_d$  for the  $d^{th}$  category is thus given by

$$F_{LBA}(\tau_d \mid \boldsymbol{\theta}_{d,s}) = 1 - \Phi(b_s/\tau_d \mid m_{d,s}, v_{d,s}),$$

where  $\boldsymbol{\theta}_{d,s} = (m_{d,s}, v_{d,s}, b_s)^T$ . The likelihood of the LBA model at the  $t^{th}$  time point is thus

$$L_t(\mathbf{y}_t \mid \mathbf{s}, \boldsymbol{\theta}) = \prod_{d=1}^{d_0} \prod_{i=1}^n \prod_{\ell=1}^{m_{i,t}} \left[ f_{LBA}(\tau_{i,\ell,t} \mid \boldsymbol{\theta}_{d,s,t}) \prod_{d' \neq d} \{1 - F_{LBA}(\tau_{i,\ell,t} \mid \boldsymbol{\theta}_{d',s,t})\} \right]^{1\{d_{i,\ell,t}=d\}},$$

where  $\boldsymbol{\theta}_{d,s,t} = (m_{d,s,t}, v_{d,s,t}, b_{s,t})^T$ , and  $f_{LBA}(\tau) = \frac{dF_{LBA}(\tau)}{d\tau}$  is the pdf of  $\tau$ .

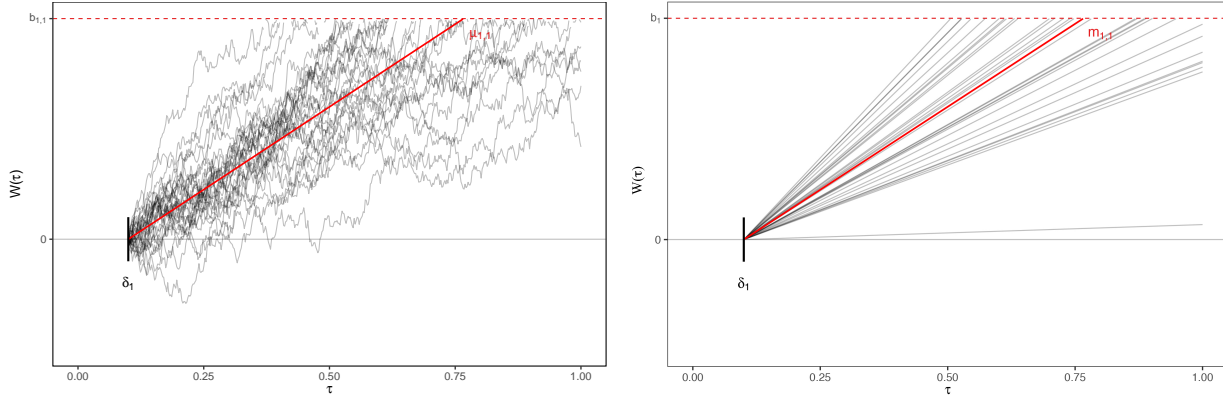


Figure S.6: Representation of the underlying evidence accumulation processes for our drift-diffusion model (left) and the LBA model (right) for 30 independent trials with fixed stimulus and decision categories  $d = s = 1$ . The red line represents the drift parameter  $\mu_{1,1}$  for the drift-diffusion model (left) and the mean of the drift parameters  $m_{1,1}$  for the LBA (right). In drift-diffusion models, trial-by-trial variability is explained by stochastically different diffusion paths for different trials. In the LBA model, trial-by-trial variability is explained by stochastically varying slopes drawn from a Normal distribution.



The existing literature on LBA models has many serious limitations. The normality assumption on the slopes  $\mu$  in the LBA model does not satisfy a non-negativity constraint. A common boundary  $b_s$  for all input stimuli  $s$  is also inflexible. Importantly, there is no principled method to incorporate systematic stimulus and decision category specific fixed or individual specific random effects into the LBA model. Existing literature is also limited to static settings, there is no mechanism to estimate smoothly varying longitudinal trajectories as the participants get trained and experienced in their decision tasks. In our implementation, we thus fitted these models separately for each time stamp. Finally, the likelihood function of the LBA model described above is non-convex in the parameters. Parameter estimation based on optimization of the likelihood function is thus fraught with convergence issues. We used the `rtdists` package (Singmann *et al.*, 2019) in R, using several random initializations and tracking the objective function to ensure convergence.

## S.7 Additional Figures

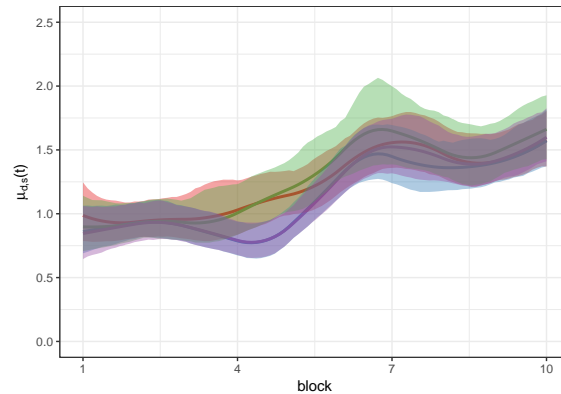


Figure S.7: Results for tone learning data: Estimated posterior mean trajectories of the population level drifts  $\mu_{d,s}(t)$  for successful identification ( $d = s$ ) of different input tones for the proposed longitudinal inverse-Gaussian drift-diffusion mixed model. The shaded areas represent corresponding 90% point wise credible intervals. Parameters for the high-flat tone response category T1 are shown in red; low-rising T2 in blue; low-dipping T3 in green; and high-falling T4 in purple.

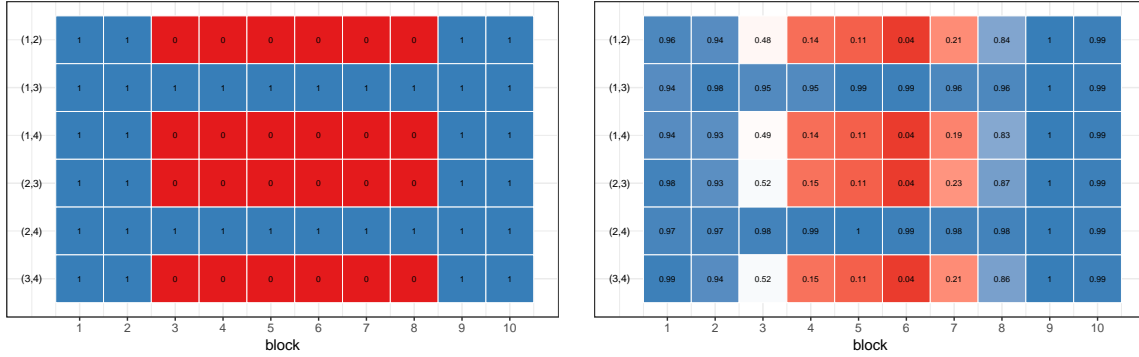


Figure S.8: Results for synthetic data: The left panel shows the true clustering structure of the underlying parameter trajectories for successful identification ( $d = s$ ) of different input tones in different learning phases. The right panel shows the corresponding posterior co-clustering probabilities estimated by our proposed method.

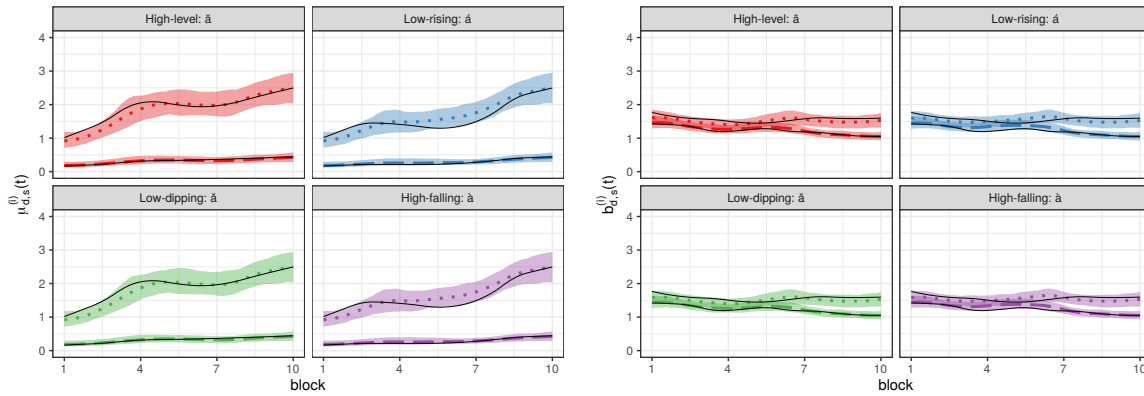


Figure S.9: Results for synthetic data: Estimated posterior mean trajectories for individual specific drifts  $\mu_{d,s}^{(i)}(t)$  (left panel) and boundaries  $b_{d,s}^{(i)}(t)$  (right panel) for two different participants - one performing well (dotted line) and one performing poorly (dashed line). The shaded areas represent corresponding 90% point wise credible intervals. The solid black lines represent underlying true curves. Parameters for the high-flat tone response category T1 are shown in red; low-rising T2 in blue; low-dipping T3 in green; and high-falling T4 in purple.

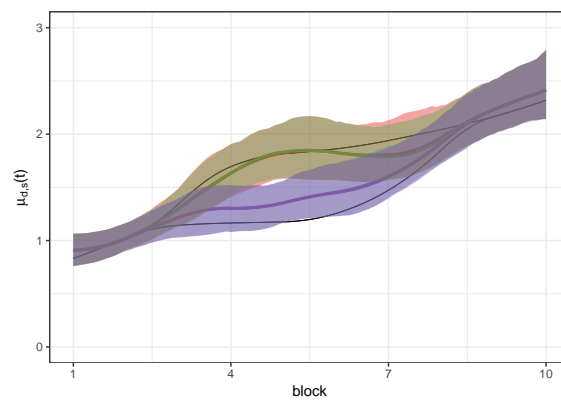


Figure S.10: Results for synthetic data: Estimated posterior mean trajectories of the population level drifts  $\mu_{d,s}(t)$  for successful identification ( $d = s$ ) of different input tones for the proposed longitudinal inverse-Gaussian drift-diffusion mixed model. The shaded areas represent corresponding 90% point wise credible intervals. The solid black lines represent underlying true curves. Parameters for the high-flat tone response category T1 are shown in red; low-rising T2 in blue; low-dipping T3 in green; and high-falling T4 in purple.

## References

- Bogacz, R., Wagenmakers, E.-J., Forstmann, B. U., and Nieuwenhuis, S. (2010). The neural basis of the speed-accuracy tradeoff. *Trends in Neurosciences*, **33**, 10–16.
- Brown, S. D. and Heathcote, A. (2008). The simplest complete model of choice response time: Linear ballistic accumulation. *Cognitive Psychology*, **57**, 153–178.
- Cavanagh, J. F., Wiecki, T. V., Cohen, M. X., Figueroa, C. M., Samanta, J., Sherman, S. J., and Frank, M. J. (2011). Subthalamic nucleus stimulation reverses mediofrontal influence over decision threshold. *Nature Neuroscience*, **14**, 1462.
- Chandrasekaran, B., Kraus, N., and Wong, P. C. (2011). Human inferior colliculus activity relates to individual differences in spoken language learning. *Journal of Neurophysiology*, **107**, 1325–1336.
- de Boor, C. (1978). *A practical guide to splines*. Springer-Verlag.
- Domenech, P. and Dreher, J.-C. (2010). Decision threshold modulation in the human brain. *Journal of Neuroscience*, **30**, 14305–14317.
- Escobar, M. D. and West, M. (1995). Bayesian density estimation and inference using mixtures. *Journal of the American Statistical Association*, **90**, 577–588.
- Feng, G., Yi, H. G., and Chandrasekaran, B. (2018). The role of the human auditory corticostriatal network in speech learning. *Cerebral Cortex*, pages 1–13.
- Forstmann, B. U., Brown, S., Dutilh, G., Neumann, J., and Wagenmakers, E.-J. (2010). The neural substrate of prior information in perceptual decision making: a model-based analysis. *Frontiers in Human Neuroscience*, **4**, 1–12.
- Frühwirth-Schnatter, S. (2006). *Finite mixture and Markov switching models*. Springer, New York.
- Ghahramani, Z. and Jordan, M. I. (1997). Factorial hidden Markov models. *Machine Learning*, **29**, 245–273.
- Giraud, A.-L. and Poeppel, D. (2012). Cortical oscillations and speech processing: Emerging computational principles and operations. *Nature Neuroscience*, **15**, 511.
- Guediche, S., Holt, L. L., Laurent, P., Lim, S.-J., and Fiez, J. A. (2014). Evidence for cerebellar contributions to adaptive plasticity in speech perception. *Cerebral Cortex*, **25**, 1867–1877.
- Hickok, G. and Poeppel, D. (2007). The cortical organization of speech processing. *Nature Reviews Neuroscience*, **8**, 393–402.

- Kennerley, S. W., Walton, M. E., Behrens, T. E., Buckley, M. J., and Rushworth, M. F. (2006). Optimal decision making and the anterior cingulate cortex. *Nature Neuroscience*, **9**, 940–947.
- Lim, S.-J., Fiez, J. A., and Holt, L. L. (2014). How may the basal ganglia contribute to auditory categorization and speech perception? *Frontiers in Neuroscience*, **8**, 1–18.
- Maddox, W. T. and Chandrasekaran, B. (2014). Tests of a dual-system model of speech category learning. *Bilingualism: Language and Cognition*, **17**, 709–728.
- McDonald, S. and Zucchini, W. (1997). *Hidden Markov and other models for discrete-valued time series*. Chapman & Hall, London.
- Mulder, M., Van Maanen, L., and Forstmann, B. (2014). Perceptual decision neurosciences—a model-based review. *Neuroscience*, **277**, 872–884.
- Neal, R. M. (2003). Slice sampling. *The Annals of Statistics*, **31**, 705–767.
- O’Doherty, J., Kringelbach, M. L., Rolls, E. T., Hornak, J., and Andrews, C. (2001). Abstract reward and punishment representations in the human orbitofrontal cortex. *Nature Neuroscience*, **4**, 95–102.
- Rabiner, L. (1989). A tutorial on hidden Markov models and selected applications in speech recognition. *IEEE*, **77**, 257–286.
- Rauschecker, J. P. and Scott, S. K. (2009). Maps and streams in the auditory cortex: Nonhuman primates illuminate human speech processing. *Nature Neuroscience*, **12**, 718–724.
- Reetzke, R., Xie, Z., Llanos, F., and Chandrasekaran, B. (2018). Tracing the trajectory of sensory plasticity across different stages of speech learning in adulthood. *Current Biology*, **28**, 1419–1427.
- Roberts, G. O. and Rosenthal, J. S. (2009). Examples of adaptive MCMC. *Journal of Computational and Graphical Statistics*, **18**, 349–367.
- Roberts, G. O., Rosenthal, J. S., *et al.* (2001). Optimal scaling for various Metropolis-Hastings algorithms. *Statistical Science*, **16**, 351–367.
- Rolls, E. T., Grabenhorst, F., and Deco, G. (2010). Choice, difficulty, and confidence in the brain. *Neuroimage*, **53**, 694–706.
- Salvata, C., Blumstein, S. E., and Myers, E. B. (2012). Speaker invariance for phonetic information: An fMRI investigation. *Language and Cognitive Processes*, **27**, 210–230.
- Scott, S. L. (2002). Bayesian methods for hidden Markov models recursive computing in the 21st century. *Journal of the American Statistical Association*, **97**, 337–351.

- Sereno, M., Pitzalis, S., and Martinez, A. (2001). Mapping of contralateral space in retinotopic coordinates by a parietal cortical area in humans. *Science*, **294**, 1350–1354.
- Singmann, H., Brown, S., Gretton, M., and Heathcote, A. (2019). rtdists: Response time distributions. R package version 0.10-0.
- Titsias, M. K. and Yau, C. (2014). Hamming ball auxiliary sampling for factorial hidden markov models. In *Advances in Neural Information Processing Systems*, pages 2960–2968.
- van Maanen, L., Brown, S. D., Eichele, T., Wagenmakers, E.-J., Ho, T., Serences, J., and Forstmann, B. U. (2011). Neural correlates of trial-to-trial fluctuations in response caution. *Journal of Neuroscience*, **31**, 17488–17495.
- Wang, Y., Spence, M. M., Jongman, A., and Sereno, J. A. (1999). Training american listeners to perceive mandarin tones. *The Journal of the Acoustical Society of America*, **106**, 3649–3658.
- White, C. N., Congdon, E., Mumford, J. A., Karlsgodt, K. H., Sabb, F. W., Freimer, N. B., London, E. D., Cannon, T. D., Bilder, R. M., and Poldrack, R. A. (2014). Decomposing decision components in the stop-signal task: a model-based approach to individual differences in inhibitory control. *Journal of Cognitive Neuroscience*, **26**, 1601–1614.
- Xie, X. and Myers, E. (2018). Left inferior frontal gyrus sensitivity to phonetic competition in receptive language processing: A comparison of clear and conversational speech. *Journal of Cognitive Neuroscience*, **30**, 267–280.
- Zanella, G. (2019). Informed proposals for local MCMC in discrete spaces. *Journal of the American Statistical Association*, pages 1–14.